Chapter III

Direct shock compression experiments on pre-molten Mg_2SiO_4 and progress towards a consistent high-pressure equation of state for CaO-MgO-Al_2O_3-SiO_2-FeO liquids

Claire W. Thomas

Paul D. Asimow

For submission to

Journal of Geophysical Research

April 4, 2013

ABSTRACT

We performed shock compression experiments on preheated forsterite liquid (Mg_2SiO_4) at an initial temperature of 2273 K and have revised the equation of state (EOS) that was previously determined by shock melting of initially solid Mg_2SiO_4 (300 K). The linear Hugoniot, U_S = 2.674±0.188 + 1.64±0.06 u_p km/s, constrains the bulk sound speed within a temperature and composition space as yet unexplored by 1-bar ultrasonic experiments. We have also revised the EOS for enstatite liquid ($MgSiO_3$) to exclude experiments that may have been only partially melted upon shock compression and also the EOS for anorthite liquid, which now excludes potentially unrelaxed experiments at low pressure. The revised fits and the previously determined EOS of fayalite and diopside were used to produce isentropes in the multicomponent CaO-MgO-Al_2O_3-SiO_2-FeO system at elevated temperatures and pressures. Our results are similar to those previously presented for peridotite and simplified "chondrite" liquids such that regardless of where crystallization first occurs, the liquidus solid sinks upon formation. This process is not conducive to the formation of a basal magma ocean. We also examined the chemical and physical plausibility of the partial melt hypothesis to explain the occurrence and characteristics of ultralow velocity zones. We determined that the ambient mantle cannot produce an equilibrium partial melt and residue that is sufficiently dense to be a ULVZ mush. The partial melt would need to be segregated from its equilibrium residue and combined with a denser solid component to achieve a sufficiently large aggregate density.

INTRODUCTION

The volumetric behavior of silicate melts at high pressures and temperatures is not well constrained despite its importance for accurately modeling the formation and early evolution of the Earth. Our ability to predict the chemical and physical consequences of the Earth's differentiation, for example, after the putative moon-forming impact, depends on a formulation of a liquid equation of state (EOS) accurate enough to determine the buoyancy of liquids relative to coexisting solids. Furthermore, the liquid EOS is also needed for rigorous interpretation of present-day deep Earth seismic observations: detection of ultra-low velocity zones (ULVZ) [*Garnero and Helmberger*, 1995] at the base of the mantle have been interpreted to possibly indicate the presence of liquid—potentially a partial melt [*Lay et al.*, 2004; *Williams et al.*, 1998] or a dense liquid that has remained un-sampled at the core-mantle boundary since differentiation of the planet [*Labrosse et al.*, 2007]. This latter idea is based in part on the simplified modeling of the mantle as an isochemical $MgSiO_3$ system [*Mosenfelder et al.*, 2009], which would begin crystallization in the mid-mantle for a full mantle magma ocean. This concept provides the potential for creating two separately evolving chemical reservoirs in the upper and lower mantle that would allow distillation of a presumed dense melt. Yet applying this same idea to slightly more complex multicomponent mantle compositions in the CaO-MgO-Al_2O_3-SiO_2-FeO (CMASF) system demonstrates that mid-mantle crystallization is not very likely or at least unlikely to lead to dynamically separate reservoirs [*Thomas et al.*, 2012]. Similarly, our current knowledge of the density differences between complex multicomponent silicate liquids and the present-day ambient mantle are not adequate to make precise predictions of the gravitational stability of a liquid-mush ULVZ.

Most of our understanding on the volume and elastic behavior of silicate liquids has been limited to pressures and temperatures within the upper mantle. Data are derived by density and sound speed measurements at 1 bar [*Ai and Lange*, 2008; *Ghiorso and Kress*, 2004; *Lange and Carmichael*, 1990] or by sink-float experiments at higher pressures up to a few GPa [*Agee*, 1992; 1993; *Ohtani et al.*, 1995; *Suzuki et al.*, 1998]. Diamond anvil cell (DAC) experiments are conducted at temperature and pressure regimes comparable to the lower mantle, but even distinguishing whether melting has occurred remains a non-trivial exercise (techniques for detecting melt vary among laboratories and results can often differ [*Andrault et al.*, 2011; *Fiquet et al.*, 2010]) and measuring the density of silicate melts *in situ* in the DAC remains an elusive goal. Shock experiments that start at ambient conditions and produce melt upon dynamic compression have achieved pressures equivalent to those in the deep mantle but can often be difficult to interpret due to solid-solid phase transitions along the Hugoniot or challenges in deciphering how far the melt reaction has been over-stepped [*Akins*, 2003; *Akins et al.*, 2004; *Luo et al.*, 2002; *Mosenfelder et al.*, 2007; *Mosenfelder et al.*, 2009].

Recently, preheated shock techniques have achieved pressures equivalent to those in the lower mantle for fully molten anorthite (An; $CaAl_2Si_2O_8$), diopside (Di; $CaMgSi_2O_6$), An_{36}-Di_{64} eutectic [*Asimow and Ahrens*, 2010], and fayalite (Fa; Fe_2SiO_4) [*Thomas et al.*, 2012] compositions. To this shock dataset of liquids we have added a series of novel experiments, which preheat Mg_2SiO_4 (forsterite, Fo) beyond its melting point at ambient conditions to 2273 K prior to dynamic compression. These experiments compliment the shock experiments performed on initially solid forsterite and wadsleyite (300K) [*Mosenfelder et al.*, 2007], and permit re-evaluation of the previous EOS without the ambiguities of distinguishing solid-melt transformations along the Hugoniot.

These experiments are also are the first to measure thermodynamic properties of Mg_2SiO_4 melt directly. The high melting temperature of forsterite (2163±20 K; [*Bowen and Andersen*, 1914]) has made *in situ* experimental measurements of melt properties difficult for this composition. They are instead typically calculated using linear mixing of partial molar properties extrapolated from lower temperatures and higher SiO_2 compositions [*Lange*, 1997; *Lange and Carmichael*, 1990; *Lange and Navrotsky*, 1992; *Stebbins et al.*, 1984]. Our newest measurements constrain the sound speed of silicate liquid within temperature and composition space yet unexplored by ambient-pressure ultrasonic experiments [*Ai and Lange*, 2008; *Ghiorso and Kress*, 2004].

METHODS

Sample Preparation of Preheated (2273 K) Shots

The Mg_2SiO_4 used for shock wave experiments was un-doped, single crystal forsterite (Morion Co. Gems) cored and lapped into disks. The sample disks under-filled the volume of the molybdenum sample holders by 7-13% at room temperature [cf. *Thomas et al.*, 2012]. The room temperature under-filling—accounting for thermal expansion of Mo and the thermal expansion and volume of fusion of forsterite—results in a 1 – 1.5 mm-deep meniscus at the top of the heated capsule at 2273 K. This bubble is above the area imaged by the streak camera and therefore still allows observation of simple one-dimensional wave propagation. A void space is preferred to over-filling of the capsule, which can result in warping or failure of the welded cap.

The surfaces within and outside the sample well including both sides of the cap were polished to a mirror finish with 1-micron alumina grit. Smoothing all the surfaces prevents bubbles from clinging to the walls of the sample holder during heating and potentially interfering with the imaged shock wave. The caps were electron-beam welded (Electron Beam Engineering

Inc., Anaheim, CA) to the sample holder wells enclosing the sample. The details of this process are described in *Thomas et al.* [2012]; we note that forsterite, unlike fayalite, welded easily with only occasional and minor oxidation of the cap.

Before and after welding, a profile of the topography aligned to the streak camera slit was taken with a depth gauge micrometer using a 0.7 mm flat-end tip. The inner portion of the sample well was measured in 0.2 mm increments, and the final driver and welded cap (or "top hat") were measured in 0.1 mm increments. Typically the topography varied no more than ±0.008mm from flat for the inside of the sample well and ±0.015mm for the outside driver and top hat. Sample capsules were carbon coated on both sides to reduce oxidation of the reflecting molybdenum surface during heating [cf. *Asimow and Ahrens,* 2010; *Asimow et al.*, 2008] except for shots completed on the 40-mm propellant gun. Oxidation of the target was less of a problem in the 40-mm gun possibly due to better vacuum for the smaller target chamber and catch tank volume compared to that of the 90mm/25mm two-stage light-gas gun (LGG).

Experimental Setup

The pioneering work for shock studies on molten materials is *Rigden et al.* [1984]. The description of our methods below builds on this and the work of *Rigden et al.* [1988; 1989], *Miller et al.* [1988; 1991a], *Chen and Ahrens* [1998], and *Chen et al.* [2002]. For more recent changes in experimental techniques and data analysis, the reader is directed to *Asimow et al.* [2008], *Asimow and Ahrens* [2010], and *Thomas et al.* [2012].

For this study, six total experiments were performed — four in the Caltech 90/25-mm two-stage LGG and two using the Caltech 40-mm propellant gun. All shots were preheated to 2000°C (2273 K) using a H_2O-cooled copper induction coil powered by a 10 kW Lepel radio frequency heater [*Chen and Ahrens,* 1998]. The targets were held in place by a "guy-wire" set up and

mounted through a hole drilled in a high-temperature Zircar™ zirconia board as opposed to the alumina board used for lower-temperature experiments [cf. *Asimow and Ahrens,* 2010].The boards were also cut with a slit from the center hole through to the bottom including two separate inch-deep slits at the top (a *Y* shape) in order to relieve mechanical stresses that arose due to thermal expansion of the board while at high temperatures. Lexan projectiles with molybdenum flyer plates (see Table 1) were used in this study; flyer plate velocities (u_{fp}) ranged from 1.04 - 5.963 km s^{-1}. For the LGG shots, u_{fp} was measured redundantly by a double-flash x-ray system and a two-magnet induction detector as described in *Asimow et al.* [2008]. The u_{fp} for the 40-mm gun shot was also measured by two methods: double-exposure x-ray image and laser cutoffs. The 40-mm x-ray system utilizes a double-flash x-ray, which doubly exposes the flyer image on a single piece of film. Velocity is determined by the separation of the two flyer images — taking into account the magnification on film and the previously calibrated parallax distance — divided by the time between the two x-ray discharges [*Rigden et al.*, 1988]. The 40-mm gun was also outfitted with a new laser timing system using 3 lasers aimed across the projectile path onto small active-area photodiode detectors. The distance between the lasers was measured to within ±0.05 cm, and the time between cutoffs is recorded on a 1 GHz oscilloscope. The velocities measured by the two techniques for each gun agreed to within the stated uncertainty for all the shots, and the average of the two values was used for the u_{fp} given in Table 1.

During each experiment, the rear face of the target was illuminated by a Specialised Imaging xenon spark lamp and filmed by a Hadland Imacon 790 streak camera through a narrow (25 μm) slit focused horizontally across the center of the driver and sample cap. The image of the shockwave transit was recorded using a new Specialised Imaging 2DR digital readout system. The system collects the streak image using a 4008 x 2688 pixel CCD, which was specifically

designed to affix to the streak camera tube. The image is captured digitally, in contrast to the previous method, which relied on digital scanning of analog images captured on Polaroid film [cf. *Asimow and Ahrens*, 2010; *Thomas et al.*, 2012]. The precise measurement of the shock transit time through the sample and molybdenum cap was measured from the extinguished (or sharp intensity change in) reflected light as the shock wave reached the free surface of the driver plate followed by the sample cap. The procedure for picking cutoffs and the calibration of the streak rate is described in *Thomas et al.* [2012]. The selected cutoffs were co-registered with the previously measured driver topography profiles and corrected for deviations from flat.

The shape of the shock front as it enters the sample is determined by interpolating the visible driver cutoffs using a 4^{th}-order polynomial. The 95% confidence interval for the fit was used as the upper and lower bounds for the location of the shock front and was the greatest source of error in the final calculated shock state — i.e., the error bars for shock pressure (P_H), shock density (ρ_H), particle velocity (u_p), and shock wave velocity (U_s). The time that the shock wave spends in the Mo cap is estimated using the iterative method of *Rigden et al.* [1988] and subtracted from the offset in time between the two cutoffs to calculate the shock wave velocity U_s in the sample. Then u_p, P_H, and ρ_H follow from impedance matching, the Rankine-Hugoniot equations, and the following input parameters: standard Hugoniot data (ρ_o, C_o, s) for the cold metal flyer and hot Mo driver plates [*Asimow et al.*, 2008; *Chase*, 1998] (see Table 2), the initial sample density (ρ_o) [*Lange*, 1997], and an initial guess for C_o and the s parameter of Mg_2SiO_4 liquid to seed the iteration (the converged result is independent of this guess).

RESULTS

Linear Hugoniot

The shock wave data for Mg_2SiO_4 liquid are reported in Table 1, including shot number, flyer/driver material, temperature prior to firing, u_{fp}, u_p, U_S, ρ_H, and P_H.

A Hugoniot is a family of peak shock states achieved in a material by progressively stronger shocks from the same starting conditions [*Ahrens*, 1987] (in this case, liquid Mg_2SiO_4 at 2273 K and 1 bar). Empirically, the Hugoniot of a well-behaved material forms a line in U_S-u_p space, given to third order in strain by $U_S = C_o + s\,u_p$ [*Jeanloz*, 1989]. The slope (s) is related to K'_S, the pressure derivative of the isentropic bulk modulus (K_{oS}) by $s = (K'_S + 1)/4$; the intercept, C_o, is the bulk sound speed of the material at room pressure ($C_o^2 = K_{oS} / \rho_o$) [*Ruoff*, 1967].

Typically, the intercept of the un-weighted linear Hugoniot in U_S-u_p space falls within error of the 1-bar value of the sound speed measured by ultrasonic techniques indicating relaxed (as opposed to "glass-like") behavior upon compression. Currently there are no 1-bar sound speed measurements on CaO-MgO-Al_2O_3-SiO_2 (CMAS) liquids with temperatures in excess of 1727K and mole fractions of MgO greater than 0.46 (Figure 1). Sound speed values can be calculated from the models of *Ghiorso and Kress* [2004] or *Ai and Lange* [2008] assuming linear addition of oxide component C_o and dC_o/dT but must be extrapolated well beyond the composition and temperature space used in either calibration (which is not recommended by the authors). The sound speed for Mg_2SiO_4 liquid at 2773K from *Ghiorso and Kress* [2004] is 3.195 km/s and from *Ai and Lange* [2008] is 3.126 km/s.

Figure 2 shows linear fits to shock data in U_S-u_p space fixed at these 1-bar model values as well as the unconstrained fit. The unconstrained, un-weighted linear fit to all preheated Mg_2SiO_4 liquid data points yields $U_S = 2.674\pm0.188 + 1.64\pm0.06\,u_p$ km/s ($r^2 = 0.995$). The unconstrained C_o falls below the derived model values potentially indicating that the dC_o/dT value is negative for Mg_2SiO_4 liquid, contrary to the positive [*Ghiorso and Kress*, 2004] and zero [*Ai and Lange*, 2008] values given in the previous studies. This is not evidence for unrelaxed behavior in the shock compression experiments; this would be expected to yield a higher bulk

modulus than expected from relaxed ultrasonic data. Instead it is evidence that the temperature or composition dependence of those models cannot be extrapolated to the current conditions; see discussion below. Consequently, the K_{oS} of 18.56±2.61 GPa (derived from the expression $K_{oS} = \rho_o C_o^2$ and the unconstrained C_o) is lower than the bulk moduli derived from either the *Ghiorso and Kress* [2004] or the *Ai and Lange* [2008] values, 26.55 and 25.38 GPa, respectively. This K_{oS} is also much lower than the previously reported value given in shock wave studies, 41 GPa at T_o=1673K [*Mosenfelder et al.*, 2009], which was derived from the *Lange and Carmichael* [1990] data set. If corrected to an initial temperature of 2273K using dV/dT and d^2V/dPdT [*Lange and Carmichael*, 1990], K_{oS} is 27.87 GPa and still much stiffer than our newest value of 18.56 GPa. The slope of our unconstrained Hugoniot fit corresponds to a K' of 5.58±0.24, compared to that of the previous estimate of 4.73 [*Thomas et al.*, 2012].

Grüneisen parameter

The thermodynamic Grüneisen parameter (γ) is a macroscopic parameter that relates thermal pressure to the thermal energy per unit volume. The Mie-Grüneisen approximation this can be expressed as

$$\gamma = \frac{1}{\rho}\frac{\partial P_{th}}{\partial E} \quad (1)$$

where thermal pressure (P_{th}) is defined as the increase in pressure due to heating at a constant volume [*Poirier*, 2000]. The Grüneisen parameter can be directly determined by the comparison of two Hugoniots with different initial densities [e.g. *Asimow and Ahrens*, 2010; *Luo et al.*, 2002]. When compared at an equal density, a liquid obtained by shock compression of an initially solid material will have a distinct pressure and internal energy state than that obtained by direct shock compression of the liquid of the same composition. This method also applies for

other changes in the initial state of shocked samples, including differences in initial solid phase and variations in initial porosity [*Mosenfelder et al.*, 2009].

We determined the Mg_2SiO_4 liquid γ by comparison of our 2273K liquid Hugoniot with the initially solid 300K forsterite Hugoniot from *Mosenfelder et al.* [2007]. *Mosenfelder et al.* used two Mg_2SiO_4 starting compositions, polycrystalline forsterite and wadsleyite, and they asserted that the two highest pressure shots from each dataset were shock melted (shots #350 and #349 forsterite and #350 and #349 wadsleyite). However, the calculations of *de Koker et al.* [2008] indicate that shock compression of crystalline forsterite along the 300K principal Hugoniot produces incongruent melting to periclase (MgO) and a more silica rich liquid in the pressure range of 150-170 GPa; only above 170 GPa is pure Mg_2SiO_4 liquid present on the calculated Hugoniot. Correspondingly, their calculated wadsleyite Hugoniot was found to be 1000-1400 K cooler than the forsterite Hugoniot. Therefore even the highest-pressure wadsleyite datum (shot #350) is unlikely to be fully molten and does not provide a secure point for evaluation of liquid properties.

We therefore have used only the highest forsterite point (#350, 188.5 GPa) from the *Mosenfelder et al.* [2007] dataset for determination of the liquid Grüneisen parameter. For the equations and details of this calculation, the reader is directed to *Asimow and Ahrens* [2010] and *Thomas et al.* [2012]. Using the power law form for γ

$$\gamma(\rho) = \left(\frac{\rho_o}{\rho}\right)^q \tag{2}$$

and

$$\gamma_o = \frac{\alpha K_{oS}}{\rho_o C_P}, \tag{3}$$

yields a q value of –1.51 and $\gamma_o = 0.448$. This corroborates the general trend that has been observed by both calculation [*Adjaoud et al.,* 2008; *Boehler and Kennedy,* 1977; *de Koker et al.,* 2008; *Stixrude and Karki,* 2005] and experiment [*Asimow and Ahrens,* 2010; *Mosenfelder et al.,* 2009; *Thomas et al.*, 2012] that liquid γ increases upon compression, opposite to the behavior of solids. This q value is also fairly similar to the Mg_2SiO_4 fit from *Thomas et al.* [2012] (which corrected a sign error in the re-fit from *Mosenfelder et al.* [2009]), but differs greatly in the value for γ_o. The difference in these fits can been seen most clearly in Figure 3, which displays the previous γ curve (dotted) and the newest fit tied at a much lower γ_o. This offset is due to the very discrepant values for K_{oS} used in (3), 41 GPa and 18.56 GPa for the previous and current study, respectively. Our newest fit for γ is also in much closer agreement to the linear fit given in *de Koker et al.* [2008] (Figure 3) and other silicate liquid γ functions derived from shock experiments.

Thermal Equation of State Fitting

The Hugoniot reaches temperatures and energies much higher than those of geophysical interest at lower mantle pressures (even for early Earth processes). It is therefore pertinent to select and apply a thermal equation of state formalism to investigate material properties that lie off the Hugoniot. We attempt to define the entire *P-V-E* surface of Mg_2SiO_4 liquid using the shock wave equation of state (SWEOS) and the 3rd- and 4th-order Birch-Murnaghan/Mie-Grüneisen equations of state (3BM/MG and 4BM/MG). The results and uncertainties for each fit are given in Table 3, and the Hugoniots are plotted in Figure 4.

The SWEOS is defined by a linear Hugoniot in $U_S - u_p$ space, converted to P - ρ space using the first and second Rankine-Hugoniot equations [e.g., *Ahrens,* 1987]. The slope of our linear Hugoniot, $U_S = 2.674 \pm 0.188 + 1.64 \pm 0.06\ u_p$ km/s, corresponds to a K'_S value of

5.58±0.24. States that lie off the Hugoniot are found using the Mie-Grüneisen thermal pressure approximation with a temperature-independent power law expression for the thermodynamic Grüneisen parameter (2). A q value of –1.51 was independently determined in the above Section 3.2 using selected experimental results from *Mosenfelder et al.* [2007].

The 3rd- or 4th-order BM/MG EOS is defined by a 3rd- or 4th-order Birch-Murnaghan isentrope centered at 1 bar and 2273K and a Mie-Grüneisen thermal pressure approximation. The 3BM/MG and 4BM/MG EOS are global fits, which include the six newest initially molten data points (Table 1) and the initially solid shot #350 forsterite from *Mosenfelder et al.* [2007]. Including the initially solid point (#350) reduces the error bars slightly for both fits; however, excluding the point returns nearly identical EOS parameters. We estimated uncertainties in these fits using bootstrap resampling of the data set; however, with only seven data points each at a distinct pressure, rather than many random samples from a population of Hugoniot constraints, this exercise yields rather artificial results.

We applied two sets of 3rd- and 4th-order BM/MG fits at T_o= 2273 K, one where K_{oS} was fixed to 18.56 GPa (derived from the unconstrained C_o) and a second where K_{oS} was permitted to vary within the stated error of the unconstrained C_o. For the first set of fits, the 3BM/MG EOS result is K_{oS}= 18.56 GPa, K'_S = 6.37±0.04, q = –2.16±0.14, and reduced χ^2 = 2.13. The 4BM/MG fit result is K_{oS}= 18.56 GPa, K'_S = 3.12±2.39, K_S" = 1.26±1.47 GPa^{-1}, q = 1.31±6.74 and reduced χ^2 = 1.18. The 4BM/MG evidently has very large error bars and strong correlations among the output parameters indicating a very unstable fitting routine. The 3BM/MG fit by contrast has less severe correlation between the parameters and appears justified by the fitting statistics.

For the second set of fits in which we allowed K_{oS} to vary, the best K_{oS} value was 16.41 GPa. This K_{oS} is the limit at which the derived C_o still yields a linear Hugoniot in U_S-u_p space.

The 3BM/MG fit with this K_{oS} value is K'_S = 7.37±0.81, q = –2.02±1.03, and reduced χ^2 = 1.65. The 4BM/MG fit is K_{oS} = 16.41 GPa, K'_S = 4.27±2.02, K_S" = 1.31±1.83 GPa^{-1}, q = 0.47±9.86, and reduced χ^2 = 1.11. This 4BM/MG fit is also unstable with large error bars and strong correlations among the parameters, but the 3BM/MG fit is much more reasonable. This 3BM/MG fit has a smaller reduced χ^2 than the 3BM/MG fit above; hence for this dataset, we prefer the 3rd-order fit with K_{oS} = 16.41 GPa.

Revised Equations of State for $MgSiO_3$ and $CaAl_2Si_2O_8$ liquids

Enstatite, $MgSiO_3$

The isentrope of $MgSiO_3$ derived from the recommended global EOS fit to shock wave data from all initial polymorphs and porosities of $MgSiO_3$ [*Mosenfelder et al.,* 2009] displays an inflection point (concave down to concave up) in *T-P* space. Although this topology is not necessarily unphysical, it conflicts with the simple concave down behavior of isentropes derived from shocked liquids only (Fa, Di, $Di_{64}An_{36}$ and Fo). It is possible that the volume decreases along the Hugoniot documented for the $MgSiO_3$ shock wave data [*Mosenfelder et al.,* 2009] may indicate that the sample is only partially molten as opposed to fully molten upon shock. Such an explanation would be consistent with the interpretation of discrepancies between shock data and MD simulations noted above for some Mg_2SiO_4 experiments [*de Koker et al.,* 2008]. However, this idea is contrary to the previous assumption that silicate minerals require such large over-stepping of the liquidus that partial melting does not occur [*Akins et al.*, 2004].

To test whether the enstatite global fit may include non-liquid data, we exclude all but six of the highest pressure points from the glass [*Mosenfelder et al.*, 2009], enstatite crystal [*Akins et al.*, 2004], oxide mix [*Marsh*, 1980], and porous [*Simakov and Trunin*, 1973] data sets. These

points are the most likely to be unambiguously molten during passage of the shock wave. The hollow points in Figure 5 shows the data used in this fit.

The resulting 4BM/MG fit yields K_{oS}= 24.66 GPa, K'_S = 10.06±0.95, K_S" = 2.34±0.82 GPa^{-1}, q= –0.88±0.68, and reduced χ^2= 1.72 at T_o = 1673.15 K. Due to the low number of points being fit, the bootstrap trial values for the output parameters for K' and q were highly correlated and were in two very distinct parameter populations — one with reasonable $q \leq 1$, and another with very high K' (~14) and unreasonably high q values (40-90). This higher set is disregarded when determining the error bars on q. This fit has a similar reduced χ^2 value to the fit given in *Mosenfelder et al.* [2009] (χ^2 = 1.89) but overall displays a simple concave down isentrope in T-P space. Although not conclusive, this result may indicate that the inflection point on the model isentrope in dT/dP space was an artifact of fitting both molten and non-molten data as opposed to showing a unique physical behavior of enstatite liquid. Therefore this result also demonstrates that the technique of detecting shock melting via significant (~3%) volume [*Akins et al.*, 2004] and temperature drops [*Luo et al.*, 2004] may not be as straightforward as previously assumed and may only indicate partial melting of silicate samples.

Anorthite, $CaAl_2Si_2O_8$

In *Thomas et al.* [2012], the anorthite and diopside liquid data of *Asimow and Ahrens* [2010] were re-analyzed only sampling the center 3 mm of the arrival top hat (see Table 1). This re-sampling was motivated by a hydro-code model of shock propagation through the capsule geometry that indicated that the outer part of the top hat arrival was influenced by edge effects. The Di EOS and the An EOS parameters were both adjusted, but only the An fit displayed an inflection point for the isentrope in T-P space. As discussed in the $MgSiO_3$ section above, it is

believed this topology is more likely an artifact of fitting non-similar experimental states as opposed to representing the actual isentropic behavior of the liquid.

The anorthite liquid Hugoniot is composed of two separate experimental data sets—one at low pressure (< 36 GPa) [*Rigden et al.*, 1989] and one at high pressure (< 126 GPa) [*Asimow and Ahrens*, 2010]. The *Rigden et al.* [1989] experiments were re-analyzed in *Asimow and Ahrens* [2010], but the C_o derived from this Hugoniot in U_S-u_p space still did not fall within error of the C_o determined in 1-bar ultrasonic measurements [*Lange and Carmichael*, 1990]. In fact, anorthite liquid is the only composition studied thus far by preheated shock wave experiments (for which an ultrasonic velocity is available at similar temperature) that displays un-relaxed behavior. In the original *Rigden et al.* study, the data was fit with two separate Hugoniots due to a sharp offset observed in U_S-u_p space for the two highest pressure points. These same data points within the 25-36 GPa range have since been interpreted to be un-relaxed during compression [*Asimow and Ahrens*, 2010; *de Koker*, 2010; *Ghiorso et al.*, 2009] despite being in the middle of the full pressure range now studied. Yet excluding these points alone does not resolve the discrepant behavior obtained by simultaneously fitting the lowest pressure points of *Ridgen et al.*, the high pressure data of *Asimow and Ahrens*, and the 1 bar bulk sound speed [*Lange and Carmichael*, 1990].

One potential reason for this discrepancy is that the two shock data sets should not actually lie on the same Hugoniot, meaning the difference in the initial temperatures for two sets of experiments may be greater than stated. The *Asimow and Ahrens* experiments were heated to initially 1932 K and measured using a pyrometer; the *Ridgen et al*. experiments ranged from 1902 K to 1919 K and were measured using a thermocouple (actual experimental temperatures of *Ridgen et al.* are published in *Asimow and Ahrens* [2010]). Typically a 30 K temperature

difference should not be significant for fitting the Hugoniot, but perhaps temperature errors using the thermocouple are larger than expected with consequently some of the experiments being conducted at significantly cooler conditions.

Other possibilities include the experiments not being held at a high enough temperature above the melting point (1826 K) or held long enough above the liquidus before firing. Finally, it is also possible that there are no experimental discrepancies but that the volumetric and elastic behavior of anorthite at low pressure may be difficult to probe due to its highly polymerized structure. The rise time for the shock may be comparable to the relaxation time at least until much stronger shocks and higher temperature conditions along the Hugoniot are achieved.

Although several plausible explanations can be put forward for the seemingly unusual character of the *Ridgen et al.* anorthite data, preliminary shock results on mixed liquids with high mole fractions of anorthite component ($An_{50}Hd_{50}$ and $An_{33}Hd_{33}Di_{33}$) (see Chapter IV), in contrast, display predictable, relaxed behavior upon compression. Although it does not provide conclusive evidence, this newest data does support the likelihood of experimental differences between the two studies as opposed to unique low-pressure behavior for anorthite liquid.

In summary, although we lack a definite understanding of the source of the low-pressure anorthite anomaly, we proceed here to derive a new fit for anorthite that can be used in conjunction with other compositions to synthesize the overall behavior of silicate liquids over a broad composition range. This is obtained from *Ridgen et al.* shot 665, the re-analyzed *Asimow and Ahrens* [2010] points [*Thomas et al.*, 2012] and the experimental 1-bar sound speed at 1932 K [*Ai and Lange*, 2008]. The parameters are for the 4BM/MG fit are K_{oS} = 19.77 GPa, K'_S = 3.72±2.14, K_S" = 0 .37±2.21 GPa^{-1}, q = –1.86±1.14, and reduced χ^2= 3.09 at T_o = 1932 K. This fit displays the same two highly correlated output parameter populations due to the low number

of points included in the fitting as seen in the $MgSiO_3$ fitting in the section above. The errors are determined using only the population of bootstrap trials with $q \leq 1$. The errors for this fit are still unavoidably large, but the fit recovers the data well and also displays a concave down isentrope in *T*-*P* space.

DISCUSSION

Sound Speed of Mg_2SiO_4 liquid

Although our derived C_o is not within the error of the 1-bar models, it is unlikely that our liquid is un-relaxed or crystallized upon compression especially at the lowest experimental pressure (9.1 GPa, see Table 1). First, it would be typical for glass-like behavior to display bulk moduli higher than the ultrasonic values [*Rivers and Carmichael*, 1987]. Although the model values are extrapolated beyond their parameter space, it is at least encouraging to observe that the liquid does not have stiffer behavior than expected from these models. Second, it has been demonstrated that crystallization during the time of the experiment is improbable since the rise time of the shock wave in the sample is much less than the time necessary for crystallization to occur [*Rigden et al.*, 1988]. Rise time (τ_r) can be estimated from

$$\tau_r = \frac{u_P \eta}{U_S \Delta P_{max}} \quad (4)$$

[*Jeanloz and Ahrens*, 1979], where η is the effective viscosity and ΔP_{max} is the maximum pressure offset between the equilibrium Hugoniot and the Rayleigh line at $P_H(U_s, u_p)$. Although η is not well constrained, the experimental 1-bar viscosity at ~2000°C for near Mg_2SiO_4 liquid composition (65.1 mol% MgO) is less than 0.1 Pa s [*Urbain et al.*, 1982]. Using conservative estimates of 0.1-3 Pa s for the change in viscosity with elevated temperature and pressure [*Adjaoud et al.*, 2008], τ_r calculated at our lowest pressure point (9.21 GPa) is on order of 10^{-10}

seconds. This rise time is more than five orders of magnitude less than the time needed for crystallization for basaltic liquids derived from the time-temperature-transformation curves given in *Uhlmann et al.* [1982] (~10^{-5} s). *Fang et al.* [1983] further show that crystallization times increase with decreased polymerization; therefore crystallization is most likely kinetically impeded on the timescales of the experimental shock in Mg_2SiO_4 liquid. Finally, the most compelling evidence that crystallization did not occur during shock compression is that the temperature-pressure path of the Hugoniot is unlikely to have crossed into the solid forsterite stability field. The Mie-Grüneisen model to estimate shock temperature (T_H) is given by

$$T_H = \frac{P_H - P_S}{\gamma C_V \rho} + T_S \quad (5)$$

where T_S and P_S are temperature and pressure along the BM isentrope, C_V is the specific heat at constant volume, and γ is the Grüneisen parameter defined as a function of volume only (1). Using the 3BM/MG EOS fit (calculated in Section 3.3), Figure 6 shows that for even the highest temperature estimates of the Mg_2SiO_4 liquidus curve [*de Koker et al.*, 2008; *Ohtani and Kumazawa*, 1981] the 2273 K Hugoniot lies within the liquid field. Consequently, we are confident that our experiments are probing relaxed liquids and that the unconstrained intercept of the linear Hugoniot of 2.674±0.188 km/s is the most accurate description of the bulk sound speed at 1 bar and 2273 K.

This result implies that the dC_o/dT for Mg_2SiO_4 is negative, i.e., sound speed decreases as temperature increases. This result is actually more in line with intuition than the previous estimates of zero [*Ai and Lange*, 2008] and positive dC_o/dT values [*Ghiorso and Kress*, 2004]. Unless there are special structural rearrangements in liquid that overcome the general tendency of materials to become more anharmonic with increasing temperature and vibrational energy, one would expect liquids to act like solids and display decreasing sounds speed as temperature

increases. Results from *de Koker et al.* [2008] also indicate a decrease in sound speed with increasing temperatures from 3000 K to 6000 K; yet extrapolation of these results to 2273 K gives a value of 3124 m/s, which does not however agree with our measured value. Preliminary modeling of this apparent complex behavior for sound speed suggests it may be due to cation coordination change and the greater degrees of structural freedom of liquids compared to solids [*Wolf et al.*, 2012].

Isentropes for full mantle magma oceans

The examination of liquidus topologies has been previously employed to describe dynamics of a solidifying magma ocean [*Andrault et al.*, 2011; *Miller et al.*, 1991b; *Mosenfelder et al.*, 2009; *Thomas et al.*, 2012]. Crystal/liquid density crossover points and isentrope-liquidus intersections are both key phenomena, and the relationship between these points is important to understand. Originally treated by *Miller et al.* [1991b], the crystallization of a chondritic (iron-depleted CI composition—see *Agee and Walker* [1988]) magma ocean was depicted as a sequence of isentropes with decreasing specific entropy (or potential temperature, T_P). The tangency of the liquid isentrope with the liquidus (maximum in S-P space) gives the pressure of first crystallization. The liquidus solid is the composition of the first forming crystal, and its density contrast with respect to the ambient liquid (whether is sinks, floats, or is neutrally buoyant) has important ramifications for understanding the first steps in the dynamic modeling of the Earth's differentiation.

The one-component liquid systems enstatite and forsterite [*Mosenfelder et al.*, 2009] have been used as compositional analogues for the mantle and exhibited deep (>80 GPa) maxima in *S-P* space. The liquidus-isentrope intersections for two multicomponent systems, KLB-1 peridotite

[*Fiquet et al.*, 2010] and synthetic chondrite [*Andrault et al.*, 2011], have also been previously examined [*Thomas et al.*, 2012]. The liquidi were taken from the above referenced studies; the details for calculating the isentropes of liquid mixtures in CaO-MgO-Al_2O_3-SiO_2-FeO composition space are given in *Thomas et al.* [2012]. Isentropes derived using the newest Mg_2SiO_4 EOS (Table 3) and other re-analyzed end-member EOS of $MgSiO_3$ and $CaAl_2Si_2O_8$ (Table 4) yield slightly different results yet similar consequences to those previously presented. The critical isentrope for simplified chondrite composition shown in Figure 7 (Ch=.62En+.24Fo+.08Fa+.04An+.02Di) has a potential temperature (T_p) of 2960 K (compared to the previous estimate of T_p =2600 K), and the intersection occurs similarly at the base of the mantle (135 GPa). The peridotite (P=.33En+.56Fo+.07Fa+.03An+.007Di) critical isentrope is T_p = 3050 K and intersects the liquidus at 105 GPa, a slightly higher temperature (T_p =2900 K) and higher pressure than previously reported (~85 GPa).

The first crystallizing phase observed on the liquidus in both experimental studies [*Andrault et al.*, 2011; *Fiquet et al.*, 2010] is Mg-perovskite ($MgSiO_3$, Pv). Using the BM3S model given in *Mosenfelder et al.* [2009] (which includes the static data of *Saxena et al.* [1999]), the density of Pv at each intersection point can be calculated to determine whether the first forming crystals would sink or float. For chondrite, the density of Pv at 135 GPa and 4690 K is 5815 kg m^{-3}, whereas chondrite liquid is 5150 kg m^{-3}. Peridotite liquid is 4874 kg m^{-3} at 105 GPa and 5035 K, but Pv is 5401 kg m^{-3}. In both cases, the liquidus solid is ~15% more dense than the liquid from which it formed and would therefore sink upon formation. This calculation can be redone to include partitioning of Fe, but current published values (D_{Fe} = 0.6 to 0.07) [*Andrault et al.*, 2012; *Nomura et al.*, 2011], which favor Fe partitioning into the liquid over high-pressure

phases, would only further increase the density difference by incorporating at least some Fe into the solid Pv to form $(Mg,Fe)SiO_3$ perovskite (MgPv).

Crystallization from the middle or base of a magma ocean has implications for potentially creating a chemically stratified early mantle [*Labrosse et al.*, 2007; *Mosenfelder et al.*, 2009] provided that the lowermost mantle were to remain molten and mechanically separated from the upper mantle [*Abe*, 1997; *Tonks and Melosh*, 1993]. It has been postulated that a dense liquid at the core-mantle boundary (CMB), isolated from convection, could serve as a location for an un-degassed, primordial reservoir, which could hold a missing budget of incompatible elements [*Labrosse et al.*, 2007; *Lee et al.*, 2010]. Yet, similar to the previous conclusion given in *Thomas et al*. [2012], because the first crystals sink upon forming, this does not support the dynamic creation of a chemically stratified mantle. This conclusion is highly dependent on the choice of composition for the early bulk mantle and the liquidus topology of that composition. As shown here, despite the simplified chondrite and peridotite liquids having very similar bulk composition, the liquidus of each composition has a different maximum in *T-P* space. This discrepancy in liquidus shape in turn gives rise to very different predictions of where crystallization would begin. It is unclear whether these very different liquidus topologies are reflective of nature or are potentially derived from the different procedures used in identifying melt in the DAC [*Andrault et al.*, 2011; *Fiquet et al.*, 2010]. Additionally, choosing a bulk earth mineralogy that was more Fe-rich than either of these compositions would result in a smaller density difference with respect to the liquid and liquidus solid, but such a composition would need to be justified theoretically with respect to the timing and sequestration of the core.

Evaluating the Partial Melt Hypothesis for Ultralow Velocity Zones

Ultra low velocity zones (ULVZs) occur in thin (5-40 km) patches above the core-mantle boundary (CMB) [*Garnero and Helmberger,* 1995]. They are distinguished by several key features, the first being that they are best fit with a 3:1 ratio of S-wave to P-wave velocity anomaly, which has been inferred to indicate of the presence of liquid [*Williams and Garnero,* 1996]. They are also discontinuous along the CMB and can be often associated with the edges of large low shear velocity provinces and the source areas of plumes and large igneous provinces [*McNamara et al.*, 2010; *Rost et al.*, 2005; *Williams et al.*, 1998]. They exhibit a non-zero shear wave velocity, so the assumed liquid cannot be present as a pure melt but must be within a liquid-solid "mush." Modeling of different melt structures for this mush permits melt fractions of 0.01 % to 30% [*Williams and Garnero,* 1996], although more than 20% could lead to the loss of structural integrity for some melt configurations [*Hernlund and Jellinek,* 2010]. At select locations where reflection coefficients have been constrained, the ULVZ is inferred to be 6-14% denser than the overlying mantle, and there is an increase in S-wave velocity with depth within the ULVZ itself [*Rost et al.*, 2006].

In order for a molten silicate liquid to comprise some portion of a ULVZ, it must be denser than or at least neutrally buoyant compared to the ambient lower-most mantle; otherwise the liquid would percolate upwards away from the CMB over geologic time. The question is whether such a melt can exist. The presence of liquid in ULVZ's as a partial melt was first inferred by *Williams and Garnero* [1996] with the assumption that the density contrast between the liquid and solid would be relatively small (~1%) so that the variations in inferred seismic velocities would be small. This idea of low density contrast is based on shock-loading experiments [*Brown et al.*, 1987; *Rigden et al.*, 1984], which showed liquid densities overtaking

their equivalent solids at moderate pressures (6-10 GPa for basaltic liquid). Figure 8 shows the densities of silicate liquids Fa, En, and Fo with major mantle solids, including periclase (Pe) and Pv, along a modern mantle adiabat (10 K/ GPa) with a T_P of 1673K. This figure indicates that the assumption of density crossovers is highly dependent on chemistry as $MgSiO_3$ liquid remains less dense than MgPv at all pressures. The density curve for each liquid in Figure 8 is shown at the base of the mantle with a range of uncertainty accounting for thermal expansion across a boundary layer for CMB temperatures of 3073-4400 K. Notably, the liquid compositions have a greater sensitivity to temperature than the solids, which is in accord with their large γ and C_V values ($\alpha = \gamma\rho C_V/K_T$). It is easy to imagine that a simple mixture of any of the liquids could produce a density comparable to that of a ULVZ. In fact Mg_2SiO_4 liquid without the additional Fe at 3073K is 10% denser than PREM [*Dziewonski and Anderson*, 1981], but the important questions are whether a chosen liquid mixture is probable both 1) chemically based on our current knowledge of lower mantle chemistry and temperatures and 2) physically based on a plausible process by which it could be produced.

There are two proposed processes for creating the putative ULVZ melt. The first is a melt left over from the differentiation of the Earth, perhaps distilled from the chemistry of the lower mantle, having been segregated from the surface by mid-mantle crystallization [*Labrosse et al.*, 2007]. A second method of producing the ULVZ melt is by partial melting of the ambient mantle. We discuss these each in turn.

As shown above, our current calculations appear to oppose segregation of a magma ocean into distinct reservoirs, but in fact our ability to constrain this problem so far applies only to the very initial stage of crystallization at the liquidus and is strongly dependent on the chosen composition. Development of a solid septum at later stages of magma ocean crystallization

cannot be entirely ruled out. In detail it remains difficult test the distillation hypothesis for chemical and physical plausibility. The liquid chemistry, initially or during progressive differentiation, could occupy a wide range of compositions within CMASF space. Furthermore, the model of *Hernlund and Jellinek* [2010] suggests that stirring of the ULVZ piles by viscous coupling to the overlying mantle could create a stable mush layer for all geologic time without ongoing melt production. This model is also rather insensitive to density contrast, requiring only that the liquid be at least slightly denser than coexisting solids and disregards any chemical interaction with the mantle. Hence it is difficult to bring much insight to bear on this model using new constraints on the composition-dependent equation of state of silicate melts.

Turning to the partial melting hypothesis, its plausibility has been supported by experiments showing that magnesiowüstite and perovskite assemblages melt at temperatures comparable to estimates for the CMB — e.g., $(Mg_{0.9},Fe_{0.1})_2SiO_4$ has a solidus temperature of 4300±270 K at 130±3 GPa [*Holland and Ahrens*, 1997]. Yet presently the melting temperatures for both Mg-Pv [*Sweeney and Heinz*, 1998; *Zerr and Boehler*, 1993] and MgO [*Asimow and Fat'yanov*, 2011] remain controversial, and the effect of Fe on the melting curve remains poorly constrained. Here, we limit our discussion to the plausibility of generating a stable ULVZ via partial melting of the ambient mantle. We will construct a model of phase and bulk densities under conditions of chemical equilibrium, which searches for an initial bulk mantle composition that would yield an equilibrium assemblage of 30% volume fraction of melt and 70% volume fraction residue that could form a gravitationally stable liquid mush (i.e., melt ≤ 1% denser than residue) with bulk density 10±4% denser than PREM (~ 6123±223 kg/m^3).

To calculate the densities of the mantle solids, (Mg, Fe)SiO_3 perovskite (MgPv) and (Mg,Fe)O ferropericlase (Fp), we used the EOS provided in *Mosenfelder et al.*[2009] for pure

Mg-Pv and pure Mg-Pe and calculated the addition of small amount of Fe^{2+} by ignoring changes in molar volume upon substitution. This is certainly an oversimplification but has already been shown to be a good approximation for estimating densities of (Mg, Fe)O solid solutions (for Fe contents up to ~60 mol%) at pressures greater than 70 GPa where Fe^{2+} is in the low-spin state and has an effective ionic radius similar to Mg^{2+} (~0.72 Å) [*Fei et al.*, 2007]. Given the low Fe contents expected in Pv solid solutions in equilibrium with melt and the substantial uncertainty that remains in the liquid EOS, this is an adequate approximation for assessment of relative melt/solid buoyancy. For calculation of liquid densities, we assume linear mixing of the oxide volumes derived from the BM/MG EOS given in Tables 3 and 4.

To define the distribution of Fe and Mg at chemical equilibrium among melt, Fp, and MgPv we need to define two partition coefficients, for example a solid-solid partition coefficient $D_{Fe}^{MgPv/Fp} = X_{Fe}^{MgPv}/X_{Fe}^{Fp}$ (where X_{Fe} is molar iron content of the phase) and one solid-melt partition coefficient $D_{Fe}^{MgPv/melt} = X_{Fe}^{MgPv}/X_{Fe}^{melt}$. The solid-solid $D_{Fe}^{MgPv/Fp}$ can be as low 0.09 [*Auzende et al.*, 2008] in Al-free systems but approaches unity for Al-bearing systems at high pressure [*Wood and Rubie*, 1996]. A similar range of experimental values exists for the solid-melt $D_{Fe}^{MgPv/melt}$ for non-Al bearing [*Nomura et al.*, 2011] (~0.07) and Al-bearing systems [*Andrault et al.*, 2012] (~0.47-0.6). We have chosen to use the values derived from high pressure Al-bearing experiments as they are likely a closer approximation to natural systems. Hence for our calculations, we assumed $D_{Fe}^{MgPv/Fp}$= 1and $D_{Fe}^{MgPv/melt}$ = 0.47 (we also explore the sensitivity of our result to this choice of solid-melt partition coefficient for Fe).

In our calculations, we also fix the SiO_2 concentration of the MgPv-Fp eutectic liquid. We chose two compositions: 1) a eutectic liquid with an SiO_2 concentration of 41 mol % such that 70% of the melt is MgPv composition (f_{pvE} = 0.7) and 30% is Fp composition and 2) a liquid

with 47 mol% SiO_2 concentration (f_{pvE} = 0.9). These two estimates bracket the eutectic composition determined by *Liebske and Frost* [2012] for the pure MgO-$MgSiO_3$ system such that SiO_2 is 44 mol % (f_{pvE} = 0.8).

Ambient mantle is often approximated as 80% (Mg, Fe)SiO_3 and 20% (Mg, Fe)O with some proportion of Fe [*Boehler*, 2000]. For our model, we evaluate whether this composition as well as other more exotic compositions would be able to produce a partial melt and an equilibrium residue with a low density contrast (a melt 1% denser than the residue, equivalent to the assumption in *Williams and Garnero* [1996]) and also produce an aggregate density comparable to a ULVZ allowing 30% volume fraction of melt.

Results for this calculation at 3700 K and 135 GPa for f_{pvE} =0.7 are given in Figure 9a. The solid lines represent curves of constant density contrast for the melt and residue, where positive percentages are a partial melt denser than the residue and negative percentages are a residue denser than the melt .The ULVZ density region is delineated by dotted lines representing a density 6-14% denser than PREM (~6123±223 kg/m^3). An estimate for ambient mantle composition of 80% MgPv +20% Fp (f_{pv} =0.8) with a Mg# of 0.85 (Mg# = $X_{Mg}/(X_{Fe}+X_{Mg})$) would produce a partial melt 5% denser than its equilibrium residue, but the aggregate density would be 5503 kg/m^3, which is actually 1% less dense than PREM. To produce an aggregate density comparable to PREM, the ULVZ bulk composition would need a very high Fe concentration (Mg# $\leq$ 0.6), but this would yield a very large (at least 14%) melt-residue density contrast. In fact for a eutectic composition of f_{pvE} =0.7 and the selected partition coefficients, there is no starting composition that can fulfill both the aggregate density and density-contrast constraints. The unphysical region on the graph represents aggregate densities that are unachievable with the given amount of Fe in the system (Mg# for the partial melt is negative

within this space). If we allow $D_{Fe}^{MgPv/melt}$ to approach unity (higher than the current experimentally determined values), thereby decreasing the extent to which Fe favors the melt and also thereby decreasing the density contrast between melt and residue, the unphysical region expands and does not permit aggregate densities within the ULVZ region. This result is also insensitive to percent of partial melting, as decreased volume fraction of melt also allows for a diminished melt-residue density contrast, but likewise further limits the highest aggregate densities that are achievable. It is an important conclusion therefore that if the eutectic composition is f_{pvE}=0.7, then there is no composition in the ternary MgO-FeO-SiO_2 system (that is, any combination of Mg# or fraction of MgPv or Fp), regardless of $D_{Fe}^{MgPv/melt}$ or melt fraction, that will produce an equilibrium assemblage equivalent to what is believed to be present in a ULVZ. In fact, this is also true for eutectic compositions f_{pvE} = 0.8 [*Liebske and Frost*, 2012] and f_{pvE} =0.9 with any experimentally determined $D_{Fe}^{MgPv/melt}$ value [*Andrault et al.*, 2011]. Only at $D_{Fe}^{MgPv/melt}$ = 0.8 and a eutectic liquid of f_{pvE} = 0.9 is the minimum estimate of the aggregate density achievable with a melt 1% denser than its residue (Figure 9b). The initial composition would also need to be exotic compared to typical ambient mantle compositions: richer in Fp (f_{pv} = 0.2 -0.5) and Fe (Mg# = 0.6-0.7).

Even disregarding the lack of experimental evidence for such high D_{Fe} or MgPv rich eutectic liquids, such high Fe contents are potentially unrealistic for a wide-spread lower mantle composition. $FeSiO_3$ is unstable in the perovskite structure and decomposes to magnesiowüstite and stishovite [*Jeanloz and Thompson*, 1983] in which case the calculations of bulk densities performed here using the MgPv EOS are no longer appropriate; although the presence of aluminum has been shown to expand both ferrous [*Kesson et al.*, 1995] and ferric stability in the perovskite and post-perovskite (pPv) phases at high pressure [*Frost and McCammon*, 2008;

Frost et al., 2008; *Zhang and Oganov*, 2006].Additionally, experiments and calculations have indicated that an Fe-rich pPv phase (with Mg# ≤ 0.8) may be stable at 130 GPa [*Mao et al.*, 2006; *Mao et al.*, 2005], yet the temperature within a ULVZ remains sufficiently under-constrained that it is unclear whether Pv or pPv would be the predominate stable phase. Similarly, although despite potentially destabilizing Pv, elevated Fe contents are likely necessary to depress the melting point of Fp to reasonable CMB temperatures, considering the melting temperature of pure MgO at ambient conditions is already very high (3060 K) [*Poirier*, 2000], granting its high pressure melting curve remains uncertain. In contrast, this partial melt calculation could yield more reasonable results with less Fe in the bulk starting composition if carried out at a lower temperature (since liquids increase in density more rapidly than solids with decreasing temperature), but at some point the conditions would drop below the solidus. The correct mantle solidus temperature is not well known and better constraints on the phase diagrams of the pertinent compositions at high pressure and temperature are needed. Therefore consequently, if the model results are correct and high Fe contents are required to produce the necessary conditions for a ULVZ, partial melting may not even be necessary as suggested in *Wicks et al.* [2010], which cites the possibility of solid-state ULVZ composed of a large proportion of Fe-rich (Fe, Mg)O to produce the observed drops in S-wave velocity.

We can conclude from this exercise that the ambient mantle (80% MgPv +20% Fp) cannot produce a partial melt and equilibrium residue that could be a ULVZ mush regardless of $D_{\mathrm{Fe}}^{\mathrm{MgPv/melt}}$ or eutectic composition. There exists a starting composition which can produce a ULVZ mush with the correct aggregate density and melt-residue density contrast, but only if subject to $D_{\mathrm{Fe}}^{\mathrm{MgPv/melt}}$ and eutectic composition constraints that lie outside of what has been determined experimentally. The partial melt hypothesis is therefore only plausible if the melt is

fractionally segregated from its residue and combined with some other denser component. Only this process would permit both an aggregate density equivalent to the bulk ULVZ mush constrained by *Rost et al.* [2006] and at the same time a have a melt-residue density contrast that is consistent with assumed values used in seismic modeling (~1%) [*Williams and Garnero*, 1996], assuming both these physical constraints are robust. And although not explicitly calculated here, another potential way to increase the aggregate density would be to transform the residue to post-perovskite structure, but partitioning of Fe in pPv is not well constrained [*Kobayashi et al.*, 2005; *Sinmyo et al.*, 2011], the location of the Pv-pPv transition in Fe-bearing systems is controversial, and it would require a special scenario to place the solid Pv-pPv transition and the onset of partial melting at the same horizon.

CONCLUSIONS

We have completed new shock wave experiments on molten Mg_2SiO_4 at 2273K, a significant technical advance in initial temperature for preheated experiments of this kind, allowing study of liquid compositions and temperatures previously inaccessible to ultrasonic or other experimental methods. This new data enables a revision of the previous liquid Mg_2SiO_4 EOS [*Mosenfelder et al.*, 2009]. The Grüneisen parameter is now in better agreement with values obtained from molecular dynamics simulation [*de Koker et al.*, 2008] and is more similar to the γ behavior of other silicate liquids such as fayalite and diopside compositions. The shock-derived ambient-pressure bulk sound speed at 2273 K, compared to values estimated from lower-temperature ultrasonic data, indicates that sound speed decreases with increasing temperature for Fo liquid, contrary to the positive [*Ghiorso and Kress*, 2004] and zero [*Ai and Lange*, 2008] temperature dependences previously reported. The EOS of liquid $MgSiO_3$ and $CaAl_2Si_2O_8$ were also revised

to exclude experiments that may have only been partially melted upon shock compression and potentially un-relaxed at low pressure, respectively, resulting in EOS models of the five components Fa, Fo, En, Di, and An that all share well-behaved, concave-down isentropes in *P-T* space. These were used in an ideal mixing model to construct new isentropes for whole mantle magma oceans of selected compositions in CMASF. The results are similar to those presented previously [*Thomas et al.*, 2012], in that MgPv may begin crystallizing in the mid-lower mantle or at the base of the mantle for different compositions or estimates of their liquidus curves but in all cases MgPv is negatively buoyant at the site of initial crystallization. This does not favor the formation of a basal magma ocean at early stages of evolution. The revised EOS of $MgSiO_3$ and Mg_2SiO_4 were also used to calculate the plausibility of producing a ULVZ from a partial melt of the ambient mantle. Results indicate that any MgPv-Fp assemblage, including compositions typically assumed for the ambient mantle (80% MgPv and 20% Fp), cannot produce an equilibrium assemblage with a density comparable to that which has been inferred for a ULVZ mush. A ULVZ must be composed of fractionally segregated liquids from elsewhere in the mantle in association with a solid component denser than the equilibrium residue.

ACKNOWLEDGEMENTS

The authors would like to thank the following: the shock wave lab technical staff—Oleg Fat'yanov, Eprapodito Gelle, and Russel Oliver. This work was supported by the National Science Foundation through award EAR-1119522.

REFERENCES

Abe, Y. (1997), Thermal and chemical evolution of the terrestrial magma ocean, *Physics of The Earth and Planetary Interiors*, *100*(1-4), 27-39.

Adjaoud, O., G. Steinle-Neumann, and S. Jahn (2008), Mg_2SiO_4 liquid under high pressure from molecular dynamics, *Chemical Geology*, *256*(3-4), 185-192.

Agee, C. B. (1992), Isothermal compression of molten Fe_2SiO_4, *Geophys. Res. Lett.*, *19*(11), 1169–1172.

Agee, C. B. (1993), Olivine flotation in mantle melt, *Earth and planetary science letters*, *114*(2-3), 315.

Agee, C. B., and D. Walker (1988), Mass balance and phase density constraints on early differentiation of chondritic mantle, *Earth and Planetary Science Letters*, *90*(2), 144-156.

Ahrens, T. J. (1987), 6. Shock Wave Techniques for Geophysics and Planetary Physics, in *Methods in Experimental Physics*, edited by G. S. Charles and L. H. Thomas, pp. 185-235, Academic Press.

Ai, Y. H., and R. A. Lange (2008), New acoustic velocity measurements on CaO-MgO-Al_2O_3-SiO_2 liquids: Reevaluation of the volume and compressibility of $CaMgSi_2O_6$-$CaAl_2Si_2O_8$ liquids to 25 GPa, *J. Geophys. Res.*, *113*(B4), B04203.

Akins, J. A. (2003), Dynamic compression of minerals in the MgO-FeO-SiO_2 system, *Ph.D. thesis, Calif. Inst. of Technol., Pasadena, Calif.*

Akins, J. A., S. N. Luo, P. D. Asimow, and T. J. Ahrens (2004), Shock-induced melting of $MgSiO_3$ perovskite and implications for melts in Earth's lowermost mantle, *Geophys. Res. Lett.*, *31*(14), L14612.

Andrault, D., N. Bolfan-Casanova, G. L. Nigro, M. A. Bouhifd, G. Garbarino, and M. Mezouar (2011), Solidus and liquidus profiles of chondritic mantle: Implication for melting of the Earth across its history, *Earth and planetary science letters*, *304*(1-2), 251-259.

Andrault, D., S. Petitgirard, G. Lo Nigro, J.-L. Devidal, G. Veronesi, G. Garbarino, and M. Mezouar (2012), Solid-liquid iron partitioning in Earth's deep mantle, *Nature*, *487*(7407), 354-357.

Asimow, P. D., and T. J. Ahrens (2010), Shock compression of liquid silicates to 125 GPa: The anorthite-diopside join, *J. Geophys. Res.*, *115*(B10), B10209.

Asimow, P. D., and O. V. Fat'yanov (2011), Pre-heated MgO shock temperature experiments require a hot melting curve, *AGU Fall Meeting Abstracts*, *1*, abstract #MR33A-08 (and the references therein).

Asimow, P. D., D. Sun, and T. J. Ahrens (2008), Shock compression of preheated molybdenum to 300 GPa, *Physics of The Earth and Planetary Interiors*, *174*(1-4), 302.

Auzende, A.-L., J. Badro, F. J. Ryerson, P. K. Weber, S. J. Fallon, A. Addad, J. Siebert, and G. Fiquet (2008), Element partitioning between magnesium silicate perovskite and ferropericlase: New insights into bulk lower-mantle geochemistry, *Earth and planetary science letters*, *269*(1–2), 164-174.

Boehler, R. (2000), High-pressure experiments and the phase diagram of lower mantle and core materials, *Rev. Geophys.*, *38*(2), 221-245.

Boehler, R., and G. C. Kennedy (1977), Pressure dependence of the thermodynamical Grüneisen parameter of fluids, *Journal of Applied Physics*, *48*(10), 4183-4186.

Bowen, N. L., and O. Andersen (1914), The binary system MgO-SiO2 *Am J Sci*, *37*, 487-500.

Brown, J. M., M. D. Furnish, and R. G. McQueen (1987), Thermodynamics for (Mg, Fe) $_2SiO_4$

from the Hugoniot, in *High Pressure Research in Mineral Physics*, edited by M. Manghnani and Y. Syono, AGU, Washington, D.C.

Chase, M. W. (1998), NIST-JANAF Thermochemical Tables, *Journal of Physical and Chemical Reference Data*, *4th edition*(Monograph 9), 1–1951.

Chen, G. Q., and T. J. Ahrens (Eds.) (1998), *Radio frequency heating coils for shock wave experiments*, 63-71 pp., Materials Research Society Symposia Proceedings, Warrendale, PA.

Chen, G. Q., T. J. Ahrens, and E. M. Stolper (2002), Shock-wave equation of state of molten and solid fayalite, *Physics of The Earth and Planetary Interiors*, *134*(1-2), 35-52.

de Koker, N. (2010), Structure, thermodynamics, and diffusion in $CaAl_2Si_2O_8$ liquid from first principles molecular dynamics, *Geochimica et Cosmochimica Acta*, *74*(19), 5657-5671.

de Koker, N., L. Stixrude, and B. B. Karki (2008), Thermodynamics, structure, dynamics, and freezing of Mg_2SiO_4 liquid at high pressure, *Geochimica et Cosmochimica Acta*, *72*(5), 1427-1441.

Dziewonski, A. M., and D. L. Anderson (1981), Preliminary reference Earth model, *Physics of The Earth and Planetary Interiors*, *25*(4), 297-356.

Fang, C. Y., H. Yinnon, and D. R. Uhlmann (1983), Cooling rates for glass containing lunar compositions, *Journal of Geophysical Research: Solid Earth*, *88*(S02), A907-A911.

Fei, Y., L. Zhang, A. Corgne, H. Watson, A. Ricolleau, Y. Meng, and V. Prakapenka (2007), Spin transition and equations of state of (Mg, Fe)O solid solutions, *Geophysical research letters*, *34*(17), L17307.

Fiquet, G., A. L. Auzende, J. Siebert, A. Corgne, H. Bureau, H. Ozawa, and G. Garbarino (2010), Melting of Peridotite to 140 Gigapascals, *Science*, *329*(5998), 1516-1518.

Frost, D. J., and C. A. McCammon (2008), The redox state of Earth's mantle, *Annual Review of Earth and Planetary Sciences*, *36*, 389-420.

Frost, D. J., U. Mann, Y. Asahara, and D. C. Rubie (2008), The redox state of the mantle during and just after core formation, *Philosophical Transactions of the Royal Society A: Mathematical, Physical and Engineering Sciences*, *366*(1883), 4315-4337.

Garnero, E. J., and D. V. Helmberger (1995), A very slow basal layer underlying large-scale low-velocity anomalies in the lower mantle beneath the Pacific: evidence from core phases, *Physics of The Earth and Planetary Interiors*, *91*(1-3), 161-176.

Ghiorso, M. S., and V. C. Kress (2004), An equation of state for silicate melts. II. Calibration of volumetric properties at 10(5) Pa, *American journal of science*, *304*(8-9), 679-751.

Ghiorso, M. S., D. Nevins, I. Cutler, and F. J. Spera (2009), Molecular dynamics studies of $CaAl_2Si_2O_8$ liquid. Part II: Equation of state and a thermodynamic model, *Geochimica et Cosmochimica Acta*, *73*(22), 6937-6951.

Hernlund, J. W., and A. M. Jellinek (2010), Dynamics and structure of a stirred partially molten ultralow-velocity zone, *Earth and planetary science letters*, *296*(1–2), 1-8.

Holland, K. G., and T. J. Ahrens (1997), Melting of $(Mg,Fe)_2SiO_4$ at the Core-Mantle Boundary of the Earth, *Science*, *275*(5306), 1623-1625.

Jeanloz, R. (1989), Shock Wave Equation of State and Finite Strain Theory, *J. Geophys. Res.*, *94*.

Jeanloz, R., and T. J. Ahrens (1979), Release adiabat measurements on minerals: The effect of viscosity, *Journal of Geophysical Research: Solid Earth*, *84*(B13), 7545-7548.

Jeanloz, R., and A. B. Thompson (1983), Phase transitions and mantle discontinuities, *Reviews of Geophysics*, *21*(1), 51-74.

Kesson, S. E., J. D. Fitz Gerald, J. M. G. Shelley, and R. L. Withers (1995), Phase relations, structure and crystal chemistry of some aluminous silicate perovskites, *Earth and planetary science letters*, *134*(1–2), 187-201.

Kobayashi, Y., T. Kondo, E. Ohtani, N. Hirao, N. Miyajima, T. Yagi, T. Nagase, and T. Kikegawa (2005), Fe-Mg partitioning between (Mg, Fe)SiO_3 post-perovskite, perovskite, and magnesiowüstite in the Earth's lower mantle, *Geophysical research letters*, *32*(19), L19301.

Labrosse, S., J. W. Hernlund, and N. Coltice (2007), A crystallizing dense magma ocean at the base of the Earth's mantle, *Nature*, *450*(7171), 866-869.

Lange, R. A. (1997), A revised model for the density and thermal expansivity of K_2O-Na_2O CaO-MgO-Al_2O_3-SiO_2 liquids from 700 to 1900 K: extension to crustal magmatic temperatures, *Contributions to Mineralogy and Petrology*, *130*(1), 1-11.

Lange, R. A., and I. S. E. Carmichael (1990), Thermodynamic properties of silicate liquids with emphasis on density, thermal expansion and compressibility, *Reviews in Mineralogy and Geochemistry*, *24*(1), 25-64.

Lange, R. A., and A. Navrotsky (1992), Heat capacities of Fe_2O_3-bearing silicate liquids, *Contributions to Mineralogy and Petrology*, *110*(2-3), 311.

Lay, T., E. J. Garnero, and Q. Williams (2004), Partial melting in a thermo-chemical boundary layer at the base of the mantle, *Physics of The Earth and Planetary Interiors*, *146*(3-4), 441-467.

Lee, C. T. A., P. Luffi, T. Hoink, J. Li, R. Dasgupta, and J. Hernlund (2010), Upside-down differentiation and generation of a 'primordial' lower mantle, *Nature*, *463*(7283), 930-U102.

Liebske, C., and D. J. Frost (2012), Melting phase relations in the MgO–$MgSiO_3$ system between 16 and 26;GPa: Implications for melting in Earth's deep interior, *Earth and planetary science letters*, *345–348*(0), 159-170.

Luo, S. N., J. L. Mosenfelder, P. D. Asimow, and T. J. Ahrens (2002), Direct shock wave loading of Stishovite to 235 GPa: Implications for perovskite stability relative to an oxide assemblage at lower mantle conditions, *Geophys. Res. Lett.*, *29*(14).

Luo, S. N., J. A. Akins, T. J. Ahrens, and P. D. Asimow (2004), Shock-compressed $MgSiO_3$ glass, enstatite, olivine, and quartz: Optical emission, temperatures, and melting, *Journal of Geophysical Research: Solid Earth*, *109*(B5), B05205.

Mao, W. L., H. Mao, W. Sturhahn, J. Zhao, V. B. Prakapenka, Y. Meng, J. Shu, Y. Fei, and R. J. Hemley (2006), Iron-Rich Post-Perovskite and the Origin of Ultralow-Velocity Zones, *Science*, *312*(5773), 564-565.

Mao, W. L., Y. Meng, G. Shen, V. B. Prakapenka, A. J. Campbell, D. L. Heinz, J. Shu, R. Caracas, R. E. Cohen, Y. Fei, R. J. Hemley, H. Mao(2005), Iron-rich silicates in the Earth's D″ layer, *Proceedings of the National Academy of Sciences of the United States of America*, *102*(28), 9751-9753.

Marsh, S. P. (Ed.) (1980), *LASL Shock Hugoniot Data* 658 pp., University of California, Berkeley.

McNamara, A. K., E. J. Garnero, and S. Rost (2010), Tracking deep mantle reservoirs with ultra low velocity zones, *Earth and planetary science letters*, *299*(1-2), 1-9.

Miller, G. H., T. J. Ahrens, and E. M. Stolper (1988), The equation of state of molybdenum at 1400 C, *Journal of Applied Physics*, *63*(9), 4469-4475.

Miller, G. H., E. M. Stolper, and T. J. Ahrens (1991a), The Equation of State of a Molten

Komatiite 1 Shock Wave Compression to 36 GPa, *J. Geophys. Res.*, *96*.
Miller, G. H., E. M. Stolper, and T. J. Ahrens (1991b), The Equation of State of a Molten Komatiite 2. Application to Komatiite Petrogenesis and the Hadean Mantle, *J. Geophys. Res.*, *96*.
Mosenfelder, J. L., P. D. Asimow, and T. J. Ahrens (2007), Thermodynamic properties of Mg_2SiO_4 liquid at ultra-high pressures from shock measurements to 200 GPa on forsterite and wadsleyite, *J. Geophys. Res.*, *112*.
Mosenfelder, J. L., P. D. Asimow, D. J. Frost, D. C. Rubie, and T. J. Ahrens (2009), The $MgSiO_3$ system at high pressure: Thermodynamic properties of perovskite, postperovskite, and melt from global inversion of shock and static compression data, *J. Geophys. Res.*, *114*.
Nomura, R., H. Ozawa, S. Tateno, K. Hirose, J. Hernlund, S. Muto, H. Ishii, and N. Hiraoka (2011), Spin crossover and iron-rich silicate melt in the Earth's deep mantle, *Nature*, *473*(7346), 199-202.
Ohtani, E., and M. Kumazawa (1981), Melting of forsterite Mg_2SiO_4 up to 15 GPa, *Physics of The Earth and Planetary Interiors*, *27*(1), 32-38.
Ohtani, E., Y. Nagata, A. Suzuki, and T. Kato (1995), Melting relations of peridotite and the density crossover in planetary mantles, *Chemical Geology*, *120*(3-4), 207-221.
Poirier, J.-P. (2000), *Introduction to the Physics of the Earth's Interior*, 2nd ed., 328 pp., Cambridge University Press, New York.
Presnall, D. C., and M. J. Walter (1993), Melting of forsterite, Mg_2SiO_4, from 9.7 to 16.5 GPa, *Journal of Geophysical Research: Solid Earth*, *98*(B11), 19777-19783.
Rigden, S. M., T. J. Ahrens, and E. M. Stolper (1984), Densities of liquid silicates at high pressures, *Science*, *226*(4678), 1071-1074.
Rigden, S. M., T. J. Ahrens, and E. M. Stolper (1988), Shock compression of molten silicate: results for a model basaltic composition, *J. Geophys. Res.*, *93*(B1), 367-382.
Rigden, S. M., T. J. Ahrens, and E. M. Stolper (1989), High-Pressure Equation of State of Molten Anorthite and Diopside, *Journal of Geophysical Research*, *94*(B7), 9508-9522.
Rivers, M. L., and I. S. E. Carmichael (1987), Ultrasonic Studies of Silicate Melts, *J. Geophys. Res.*, *92*(B9), 9247-9270.
Rost, S., E. J. Garnero, and Q. Williams (2006), Fine-scale ultralow-velocity zone structure from high-frequency seismic array data, *J. Geophys. Res.*, *111*(B9), B09310.
Rost, S., E. J. Garnero, Q. Williams, and M. Manga (2005), Seismological constraints on a possible plume root at the core-mantle boundary, *Nature*, *435*(7042), 666-669.
Ruoff, A. (1967), Linear Shock-Velocity-Particle-Velocity Relationship, *Journal of Applied Physics*, *38*(13), 4976.
Saxena, S. K., L. S. Dubrovinsky, F. Tutti, and T. Le Bihan (1999), Equation of state of $MgSiO_3$ with the perovskite structure based on experimental measurement, *American Mineralogist*, *84*(3), 226-232.
Simakov, G. V., and R. F. Trunin (1973), On the existence of overdense perovskite structures in magnesium silicates under conditions of high pressure (English translation), *Izvestiya Earth Phys*, *9*, 603-604.
Sinmyo, R., K. Hirose, S. Muto, Y. Ohishi, and A. Yasuhara (2011), The valence state and partitioning of iron in the Earth's lowermost mantle, *J. Geophys. Res.*, *116*(B7), B07205.
Stebbins, J. F., I. S. E. Carmichael, and L. K. Moret (1984), Heat capacities and entropies of silicate liquids and glasses, *Contributions to Mineralogy and Petrology*, *86*(2), 131-148.
Stixrude, L., and B. Karki (2005), Structure and Freezing of $MgSiO_3$ Liquid in Earth's Lower

Mantle, *Science*, *310*(5746), 297-299.
Stixrude, L., and C. Lithgow-Bertelloni (2005), Thermodynamics of mantle minerals – I. Physical properties, *Geophysical Journal International*, *162*(2), 610-632.
Suzuki, A., E. Ohtani, and T. Kato (1998), Density and thermal expansion of a peridotite melt at high pressure, *Physics of The Earth and Planetary Interiors*, *107*(1–3), 53-61.
Sweeney, J. S., and D. L. Heinz (1998), Laser-heating through a diamond-anvil cell: Melting at high pressures, in *Properties of Earth and Planetary Materials at High Pressure and Temperature*, edited by M. H. Manghanani and T. Yagi, pp. 197-214, Geophysical Monograph-American Geophysical Union, Washington D.C.
Thomas, C. W., Q. Liu, C. B. Agee, P. D. Asimow, and R. A. Lange (2012), Multi-technique equation of state for Fe_2SiO_4 melt and the density of Fe-bearing silicate melts from 0 to 161 GPa, *J. Geophys. Res.*, *117*(B10), B10206.
Tonks, W. B., and H. J. Melosh (1993), Magma Ocean Formation Due to Giant Impacts, *J. Geophys. Res.*, *98*(E3), 5319-5333.
Uhlmann, D. R., H. Yinnon, and C.-Y. Fang (1982), Simplified model evaluation of cooling rates for glass-containing lunar compositions, *Lunar and Planetary Science Conference*, *12B*, 281-288.
Urbain, G., Y. Bottinga, and P. Richet (1982), Viscosity of liquid silica, silicates and alumino silicates, *Geochimica et Cosmochimica Acta*, *46*(6), 1061-1072.
Wicks, J. K., J. M. Jackson, and W. Sturhahn (2010), Very low sound velocities in iron-rich (Mg, Fe) O: Implications for the core-mantle boundary region, *Geophysical research letters*, *37*(15), 15304.
Williams, Q., and E. J. Garnero (1996), Seismic Evidence for Partial Melt at the Base of Earth's Mantle, *Science*, *273*(5281), 1528-1530.
Williams, Q., J. Revenaugh, and E. J. Garnero (1998), A Correlation Between Ultra-Low Basal Velocities in the Mantle and Hot Spots, *Science*, *281*(5376), 546-549.
Wolf, A. S., P. D. Asimow, and D. J. Stevenson (2012), A Simplified Cation Speciation Model for Silicate Liquids at Mantle Pressures and Temperatures, *AGU Fall Meeting Abstracts*, *1*, abstract MR43A-2300.
Wood, B. J., and D. C. Rubie (1996), The Effect of Alumina on Phase Transformations at the 660-Kilometer Discontinuity from Fe-Mg Partitioning Experiments, *Science*, *273*(5281), 1522-1524.
Zerr, A., and R. Boehler (1993), Melting of $(Mg,Fe)SiO_3$ Perovskite to 625 Kilobars: Indication of a High Melting Temperature in the Lower Mantle, *Science*, *262*(5133), 553-555.
Zhang, F. W., and A. R. Oganov (2006), Mechanisms of Al^{3+} incorporation in $MgSiO_3$ post-perovskite at high pressures, *Earth and planetary science letters*, *248*(1-2), 69-76.

Table 1. Shock compression data

Shot #	Flyer material	T (K)	u_{fp} km s^{-1}		u_p km s^{-1}		U_s km s^{-1}		ρ_H Mg m^{-3}		P_H GPa	
Forsterite												
1075 [a]	Mo	2274	2.019	0.003	1.644	0.001	5.38	0.02	3.74	0.01	22.98	0.07
1077 [a]	Mo	2273	1.04	0.02	0.886	0.004	4.00	0.11	3.34	0.03	9.21	0.2
455	Mo	2273	5.426	0.007	4.08	0.02	9.14	0.17	4.68	0.09	96.7	1.4
457	Mo	2273	3.32	0.01	2.59	0.03	7.10	0.44	4.10	0.17	47.6	2.3
458	Mo	2273	4.522	0.008	3.41	0.01	8.47	0.12	5.29	0.05	75.0	0.8
459	Mo	2273	5.964	0.002	4.43	0.02	9.95	0.17	5.42	0.08	114.3	1.5
Anorthite												
665†	Cu	1922.2	1.8	0.03	1.325	0.025	4.68	0.01	3.57	0.03	15.90	0.30
364	Mo	1930	4.997	0.005	3.816	0.003	8.49	0.04	4.64	0.02	82.80	0.28
380	Mo	1932	5.434	0.003	4.501	0.005	9.56	0.05	4.84	0.03	95.30	0.63
379	Mo	1932	6.007	0.025	4.094	0.007	9.09	0.08	4.66	0.04	110.00	0.44
382	Mo	1932	6.533	0.013	4.868	0.024	10.06	0.23	4.97	0.13	126.00	2.30
Diopside												
	Mo	1781	4.984	0.003	3.697	.008	9.33	0.10	4.34	0.03	90.84	0.72

[a] Caltech 40mm propellant gun † Anorthite and diopside shots are from *Asimow and Ahrens* [2010] revised in *Thomas et al.* [2012] but not previously published except for 665 which was revised in *Asimow and Ahrens* [2010] and originally from *Rigden et al.* [1989].

Table 2. Parameters used

		Molybdenum (2273 K)	Molybdenum (300 K)
ρ_o	Mg m^{-3}	9.785	10.21
C_o	km s^{-1}	4.858	5.033
s		1.288	1.289

Asimow et al. [2008]; *Chase* [1998]

Table 3. Equation of State fits for molten Mg_2SiO_4

	Units	SWEOS	BM3	BM4	Source
T_o	K	2273	2273	2273	
ρ_o	kg m^{-3}	2597 9 11	2597 ± 11	2597 ± 11	L97
C_o	m s^{-1}	2674 ± 19	-	-	fitted
s		1.64 ± 0.06	-	-	fitted
γ_o		0.448	0.396	0.396	derived
q		-1.51†	–2.02 ± 1.03	0.47 ± 9.86	fitted
K_{oS}	GPa	18.57	16.41*	16.41*	derived/*fitted
K_S'		5.58 ± 0.24	7.37 ± 0.81*	4.27 ± 2.02*	derived/*fitted
K_S''	GPa^{-1}	-	-	1.31 ± 1.83	fitted
χ^2		-	1.65	1.11	
K_T	GPa	16.54	14.80	14.80	derived
α	K^{-1}	1.21-04	1.21-04	1.21-04	L97
C_p	J kg^{-1}	1926.18	1926.18	1926.18	LN92
C_v	J kg^{-1}	1715.23	1737.36	1737.36	derived

SWEOS= shock wave equation of state. 3BM/MG = 3rd-order Birch-Murnaghan/Mie-Grüneisen EOS 4BM/MG = 4th-order Birch-Murnaghan/Mie-Grüneisen EOS. † derived from shot 350 Fo *Mosenfelder et al.* [2007] Sources: *Fitted* indicates an adjustable parameter, L97 is *Lange* [1997], LN92 is *Lange and Navrotsky* [1992]

Table 4. Equation of State fits for molten silicate liquids

	Units	3BM/MG Di†	3BM/MG Fa†	4BM/MG An	4BM/MG En	Source
T_o	K	1673	1573	1932	1673	
ρ_o	kg m^{-3}	2643	3699	2560	2617	L97
γ_o		0.493	0.412	0.174	0.365	derived
q		-1.28	-0.95	-1.86	-0.88	fitted
K_{oS}	GPa	24.57	21.99	19.77	24.66	derived
K_S'		6.77	7.28	3.73	10.07	fitted
K_S''	GPa^{-1}	-	-	0.38	-2.35	fitted
C_p	J kg^{-1} K^{-1}	1612.56	1182.35	1528.72	1761.15	LN92
C_v	J kg^{-1} K^{-1}	1506.21	1122.73	1511.28	1690.53	derived

3BM/MG = 3rd-order Birch-Murnaghan/Mie-Grüneisen EOS 4BM/MG = 4th-order/Birch-Murnaghan Mie-Grüneisen EOS. Sources: *Fitted* indicates an adjustable parameter, L97 is *Lange* [1997], LN92 is *Lange and Navrotsky* [1992], †Thomas et al [2012]

FIGURE CAPTIONS

Figure 1. The set of experiments used for modeling sound speeds of silicate liquids in *Ghiorso and Kress* [2004] and *Ai and Lange*[2008] compared to the initial temperature and composition of Mg_2SiO_4 liquid.

Figure 2. Preheated (2273K) forsterite Hugoniot in shock velocity (U_s)-particle velocity (u_p) space. The thick black line represents the unconstrained linear Hugoniot; the orange and blue lines are fixed at the sound speeds calculated using the models from *Ghiorso and Kress* [2004] and *Ai and Lange*[2008], respectively.

Figure 3. The behavior of Grüneisen parameter for Mg_2SiO_4 liquid (thick solid green) compared to its previously reported value (dotted) [*Mosenfelder et al.*, 2009]. The thin red and blue lines are the behavior of γ for diopside and fayalite, respectively. The EOS parameters used are given in Table 4. The squares and black line and are the results and linear fit from MD simulations of Mg_2SiO_4 liquid [*de Koker et al.*, 2008]

Figure 4. Mg_2SiO_4 liquid Hugoniot plotted in pressure-density space with thermal EOS fits. Data symbols are the same as Figure 3. Abbreviations: SWEOS- shock wave equation of state; BM/MG – Birch-Murnaghan/Mie-Grüneisen EOS

Figure 5. $MgSiO_3$ Hugoniot data used in the global fit of *Mosenfelder et al*. [2009] for $MgSiO_3$ melt. The volume for each experimental point is normalized to the volume of its starting

material. The data set includes enstatite glass [*Mosenfelder et al.*, 2009] (triangle), enstatite crystal [*Akins et al.*, 2004] (diamond), oxide mix [*Marsh*, 1980] (circle), and porous enstatite [*Simakov and Trunin*, 1973] (square). The gray line is the high pressure state assignment from *Mosenfelder et al*. [2009] to either perovskite, post-perovskite, or melt. Only the hollow points were included in our fit. Solid points within the melt field were excluded. Error bars not shown.

Figure 6. Estimates of the Mg_2SiO_4 liquidus from *de Koker et al.* [2008] (black curve with shaded gray error), *Presnall and Walter* [1993](green curve) and *Ohtani and Kumazawa* [1981] purple curve including the experimentally determinations liquid (circles) and solid (squares) quench. The estimated *T*-*P* path of the Hugoniot (dashed line) and shot #1077 (diamond) (see Table 1) lie within the liquid field.

Figure 7. Models for the early mantle upon cooling showing the comparison of the liquidus curves (black solid line) with the isentropic temperature profile (dotted line) of the same composition. (a) Simplified “chondritic” composition and liquidus from *Andrault et al.* [2011]. (b) Peridotite KLB-1 composition and liquidus from *Fiquet et al.* [2010]. The critical isentrope with its mantle potential temperature is shown in red. The tangent point of the critical isentrope and the liquidus gives the pressure and temperature at the onset of crystallization. The EOS parameters used for calculating the isentropes are given in Table 3 and 4.

Figure 8. Estimated densities for silicate liquids Fa (blue curve), Fo (green curve) and En (orange curve) and mantle solids Fo, wadsleyite (Wd), ringwoodite (Rw), periclase (Pe), Mg-perovskite (Pv), and post-perovskite (pPv) (black curves) as function of pressure along a 10K/GPa mantle

geotherm. The dashed lines are the previous density estimates for Fo liquid (green) and En liquid (orange) from EOS parameters given in *Mosenfelder* et al. [2009].The density at base of mantle (135 GPa) for each composition is thermally corrected from 3073K to 4400K (shaded cones). Also shown is the density profile from PREM [*Dziewonski and Anderson*, 1981], the inferred density for a ULVZ from seismic reflection coefficients [*Rost et al.*, 2006](square), and an estimated ambient mantle composition of 80% $(Mg_{0.85}Fe_{0.15})SiO_3$ perovskite+ 20% $(Mg_{0.85}Fe_{0.15})O$ (diamond) at 3000K and 129 GPa. The EOS parameters for the liquids are taken from Tables 3 and 4. EOS for Mg-Pv and pPv are from *Mosenfelder* et al. [2009]; other solid EOS are from *Stixrude and Lithgow-Bertelloni* [2005].

Figure 9. Results for partial melting calculation at 3700 K and 135 GPa. The solid curves represent lines of constant density contrast for the melt and residue, where positive percentages are a partial melt denser than the residue and negative percentages are a residue denser than the melt for a given starting composition. The y-axis if the fraction of MgPv in the starting material (f_{pv}) where the remainder is Fp; the x-axis is the Mg# of the starting composition, where Mg#.= $X_{Mg}/(X_{Fe}+X_{Mg})$.The density of the ULVZ is the blue region delineated by dotted lines representing a density 6-14% denser than PREM (~6123±223 kg/m^3). An estimate for ambient mantle composition of 80% MgPv +20% Fp (f_{pv} =0.8) with an Mg# of 0.85 is given with its calculated aggregate density (agg ρ) with 30% volume fraction of partial melt. The unphysical region on the graph signifies where Mg# for the partial melt is negative and hence represents aggregate densities that are unachievable with the given amount of Fe in the system) The eutectic liquid is fixed at 70% MgPv (f_{pvE} = 0.7) and the $D_{Fe}^{MgPv/melt}$ = 0.47. b) The eutectic liquid is fixed at 90% MgPv (f_{pvE} = 0.97) and the $D_{Fe}^{MgPv/melt}$ = 0.8.

FIGURES

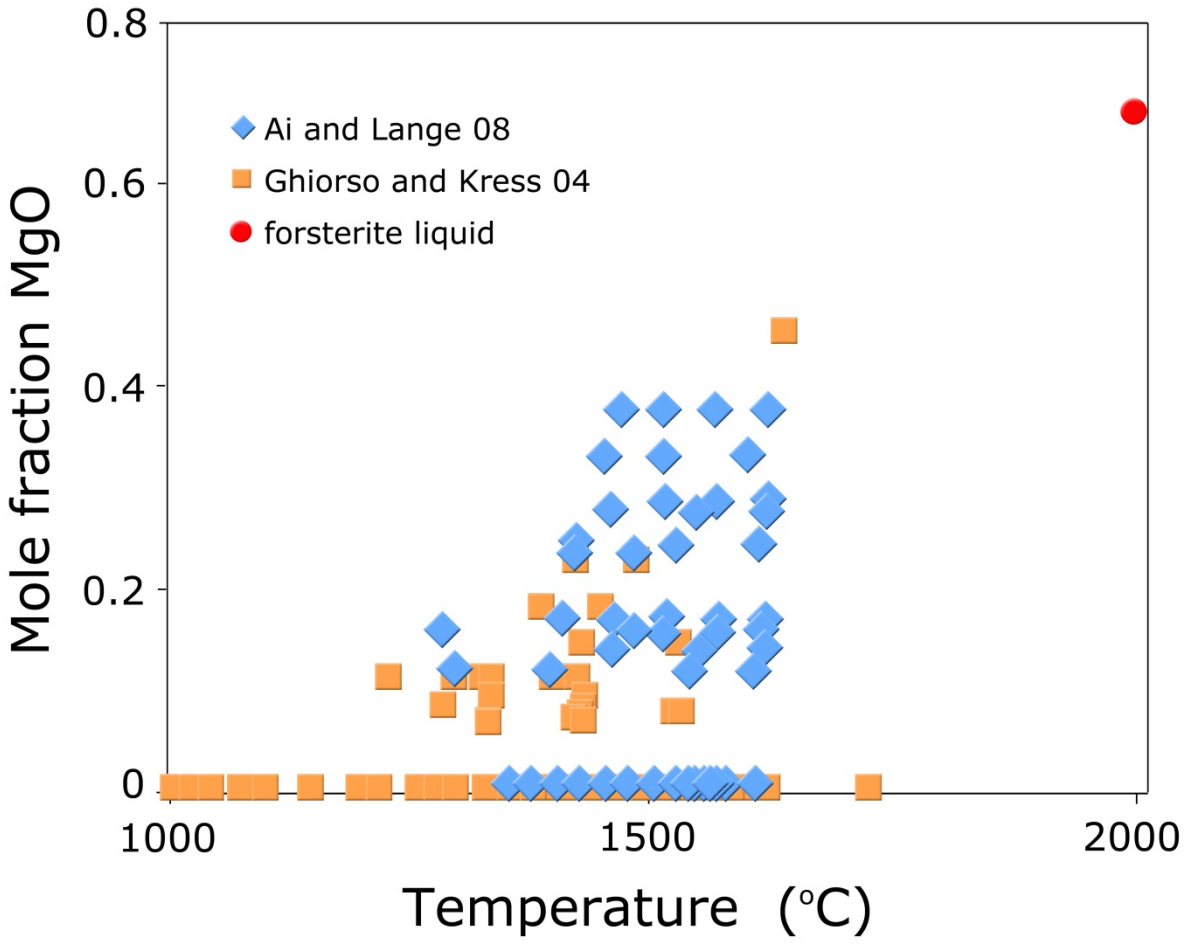

Figure 1

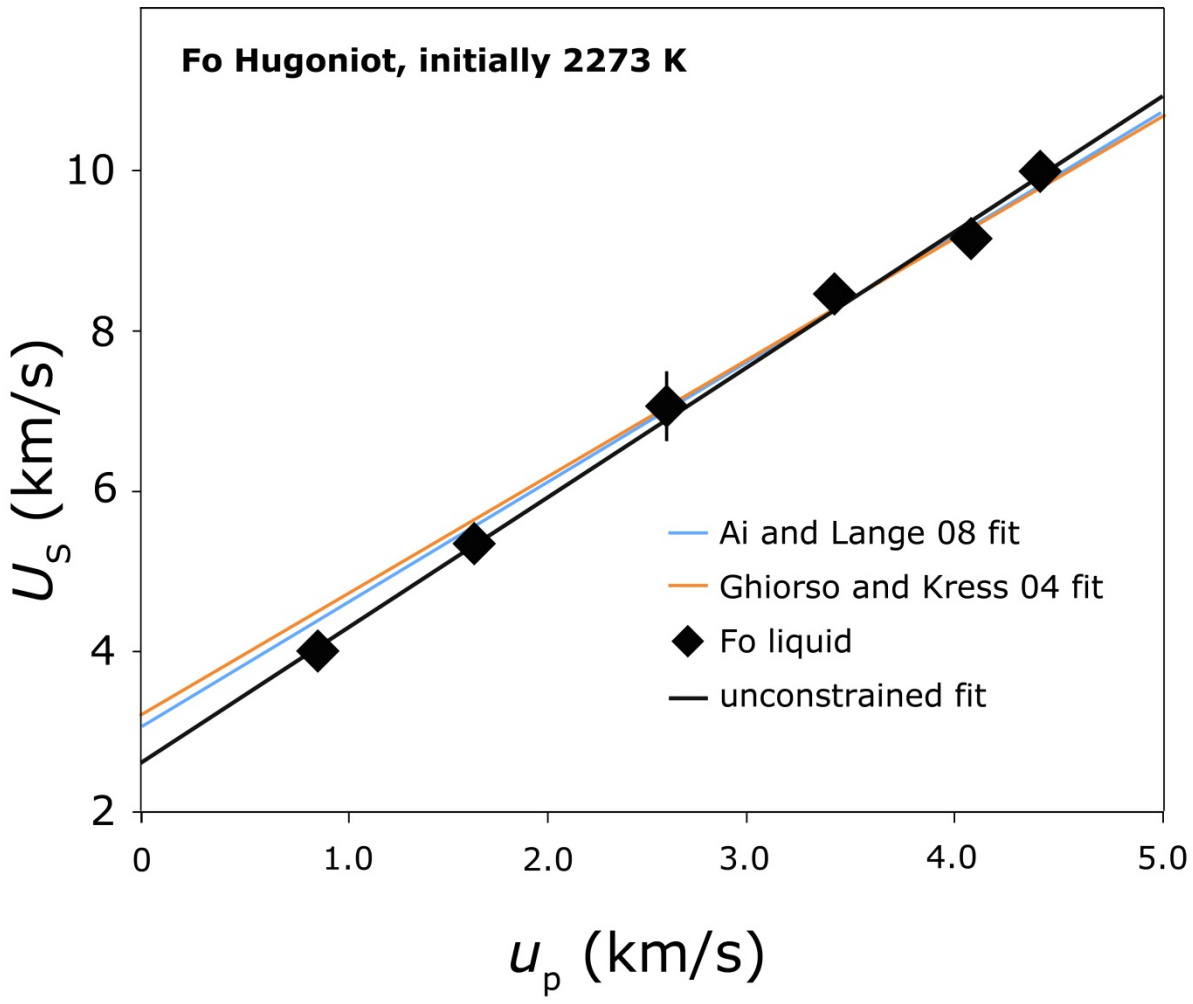
Fo Hugoniot, initially 2273 K
10
8
6
4
2
U_S (km/s)
0
1.0
2.0
3.0
4.0
5.0
u_p (km/s)
Ai and Lange 08 fit
Ghiorso and Kress 04 fit
Fo liquid
unconstrained fit

Figure 2

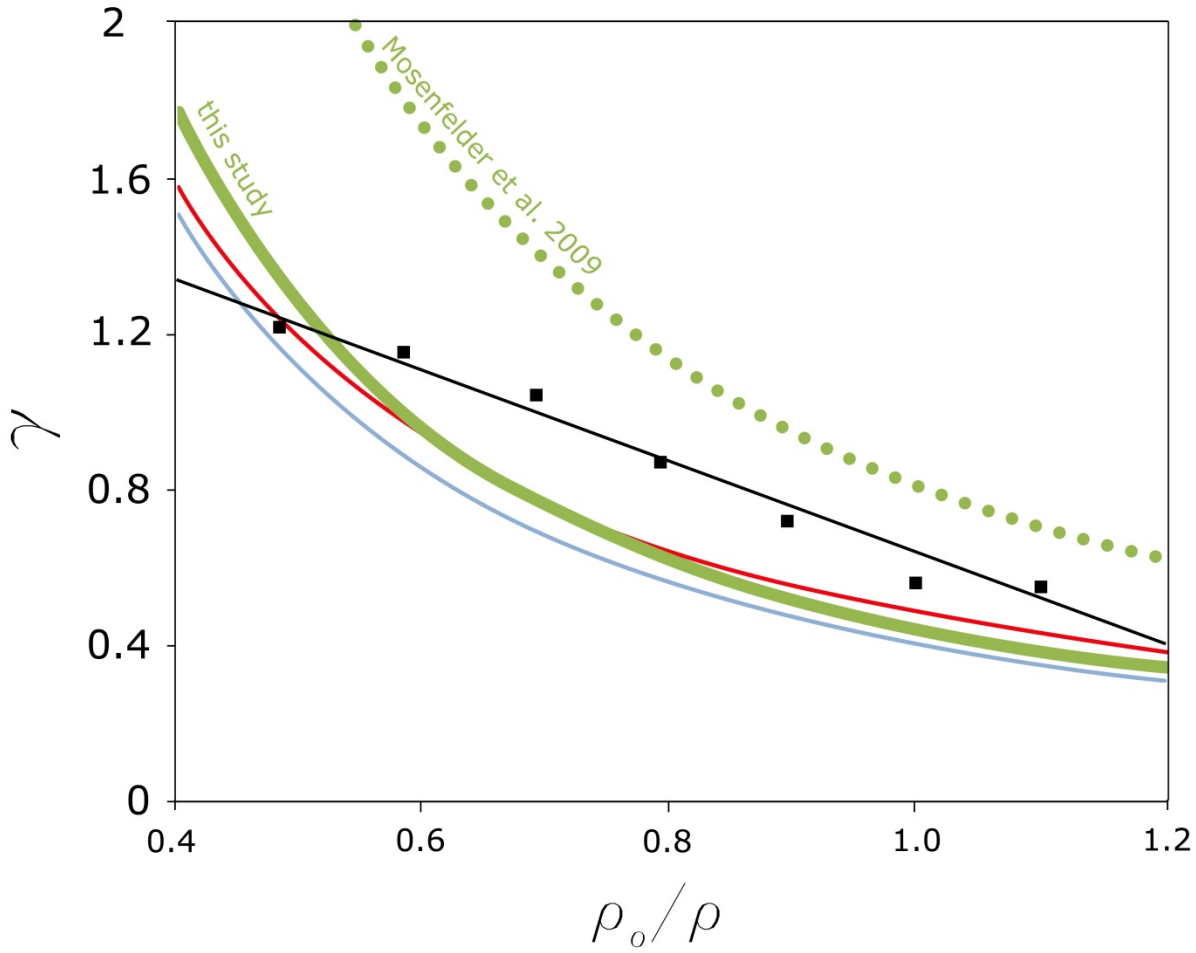
2
1.6
1.2
0.8
0.4
0
0.4
0.6
0.8
1.0
1.2
γ
ρ_o/ρ
this study
Mosenfelder et al. 2009

Figure 3

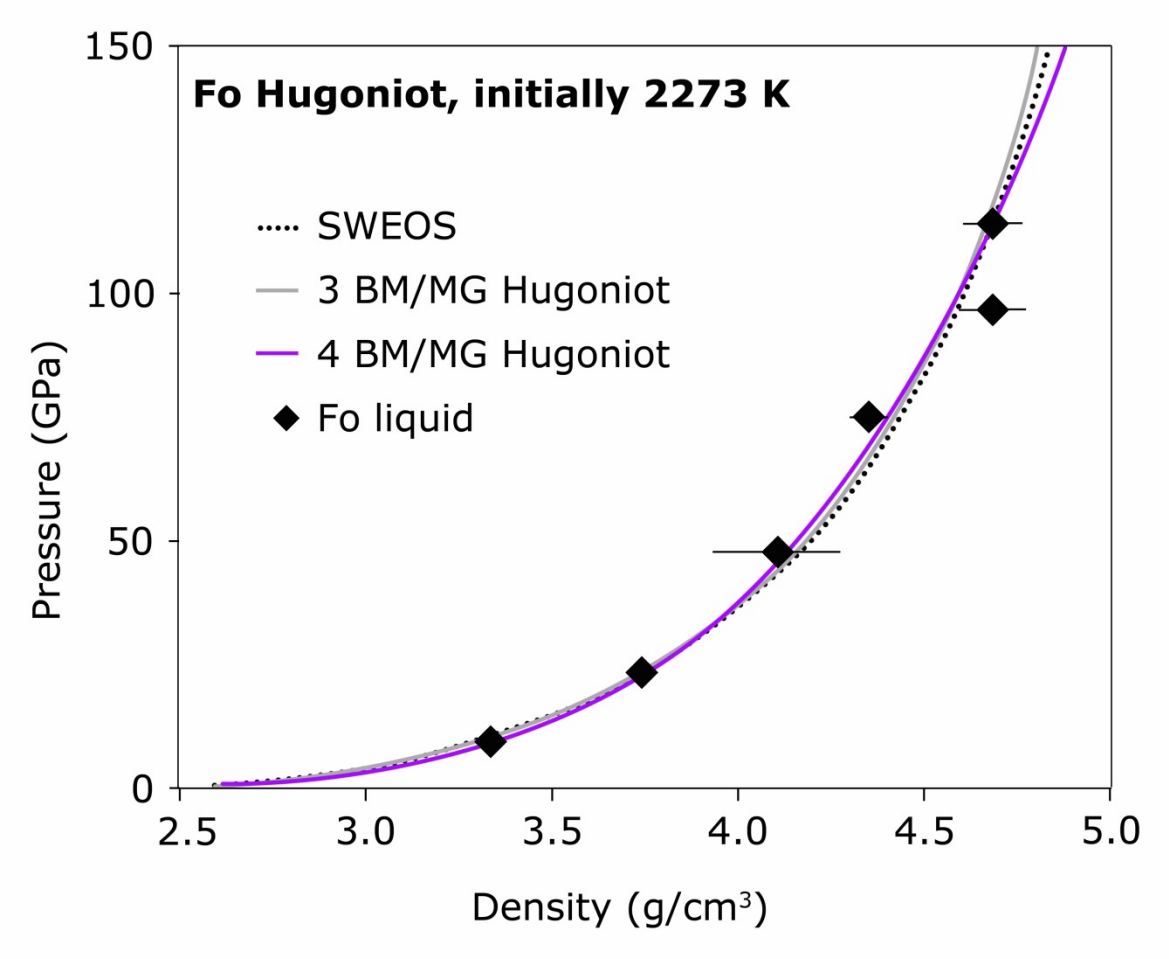
Fo Hugoniot, initially 2273 K
SWEOS
3 BM/MG Hugoniot
4 BM/MG Hugoniot
Fo liquid
Pressure (GPa)
Density (g/cm³)
150
100
50
0
2.5
3.0
3.5
4.0
4.5
5.0

Figure 4

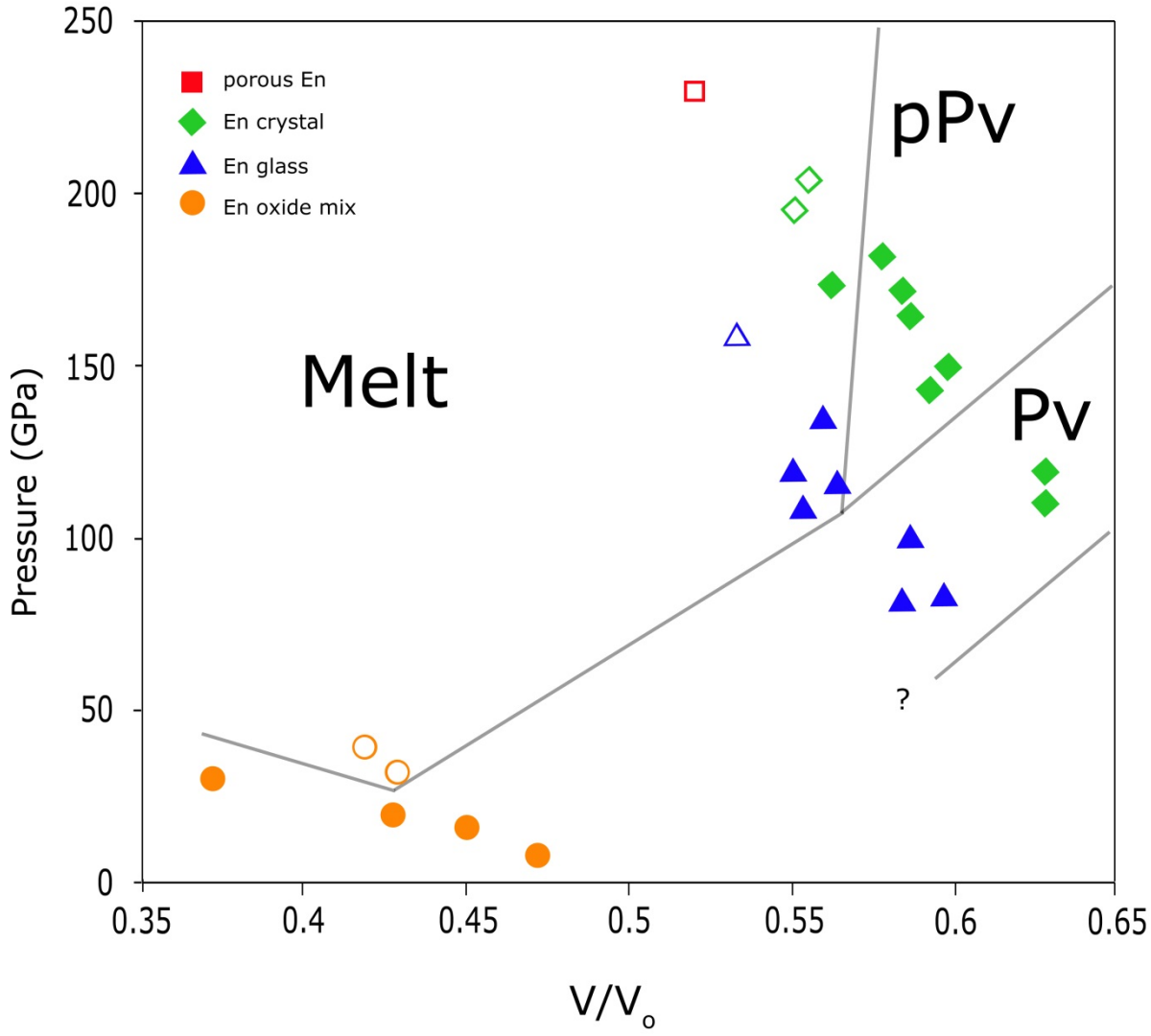
porous En
En crystal
En glass
En oxide mix
Melt
pPv
Pv
?
Pressure (GPa)
V/V$_o$
250
200
150
100
50
0
0.35
0.4
0.45
0.5
0.55
0.6
0.65

Figure 5

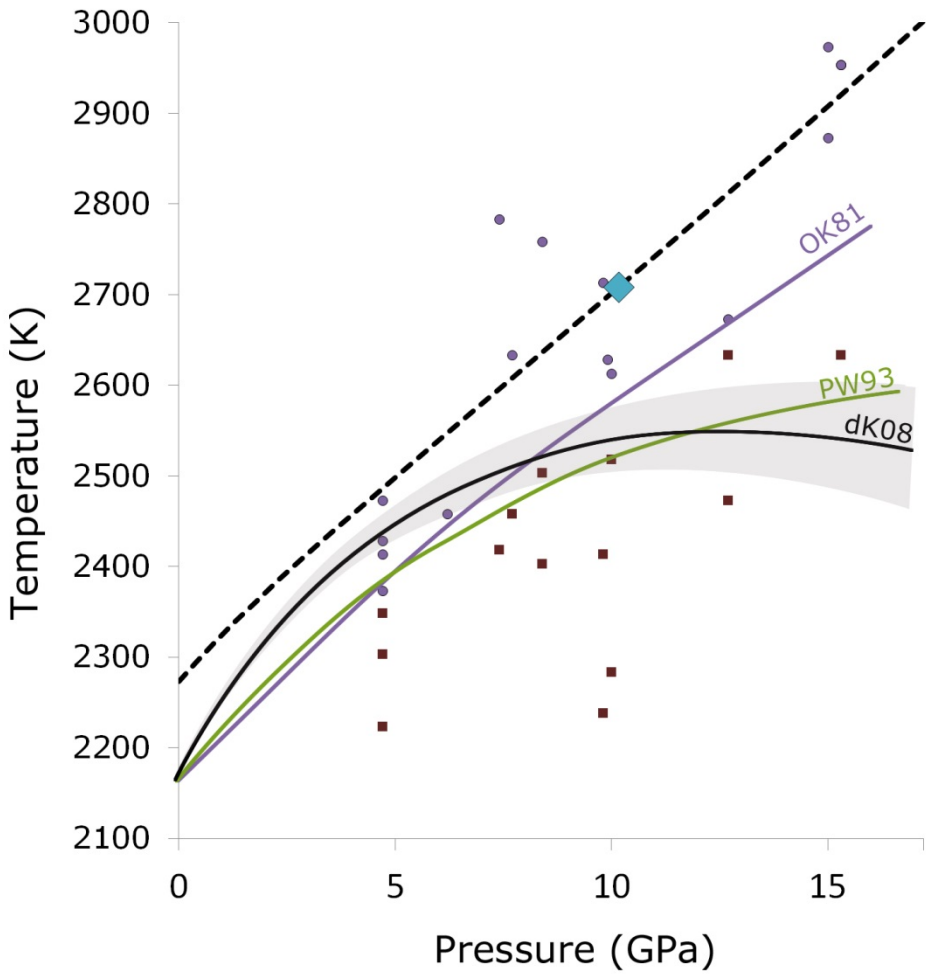
3000
2900
2800
2700
2600
2500
2400
2300
2200
2100
Temperature (K)
0
5
10
15
Pressure (GPa)
OK81
PW93
dK08

Figure 6

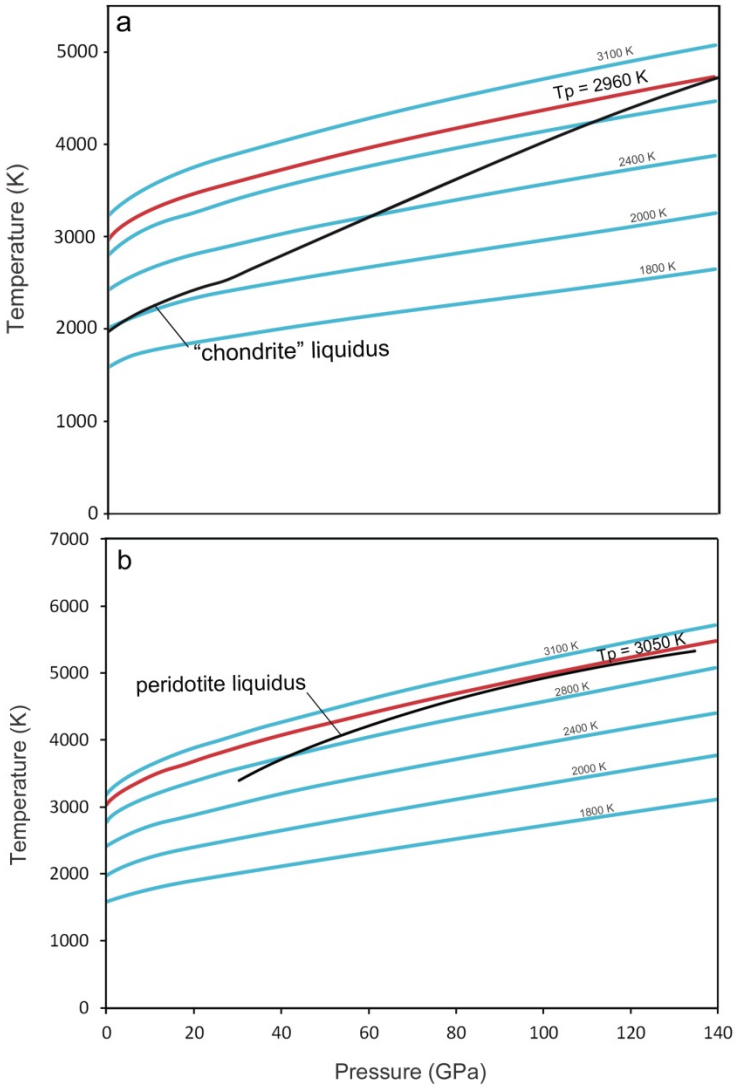
a
3100 K
Tp = 2960 K
2400 K
2000 K
1800 K
"chondrite" liquidus
Temperature (K)
0
1000
2000
3000
4000
5000
b
3100 K
Tp = 3050 K
peridotite liquidus
2800 K
2400 K
2000 K
1800 K
Temperature (K)
0
1000
2000
3000
4000
5000
6000
7000
0
20
40
60
80
100
120
140
Pressure (GPa)

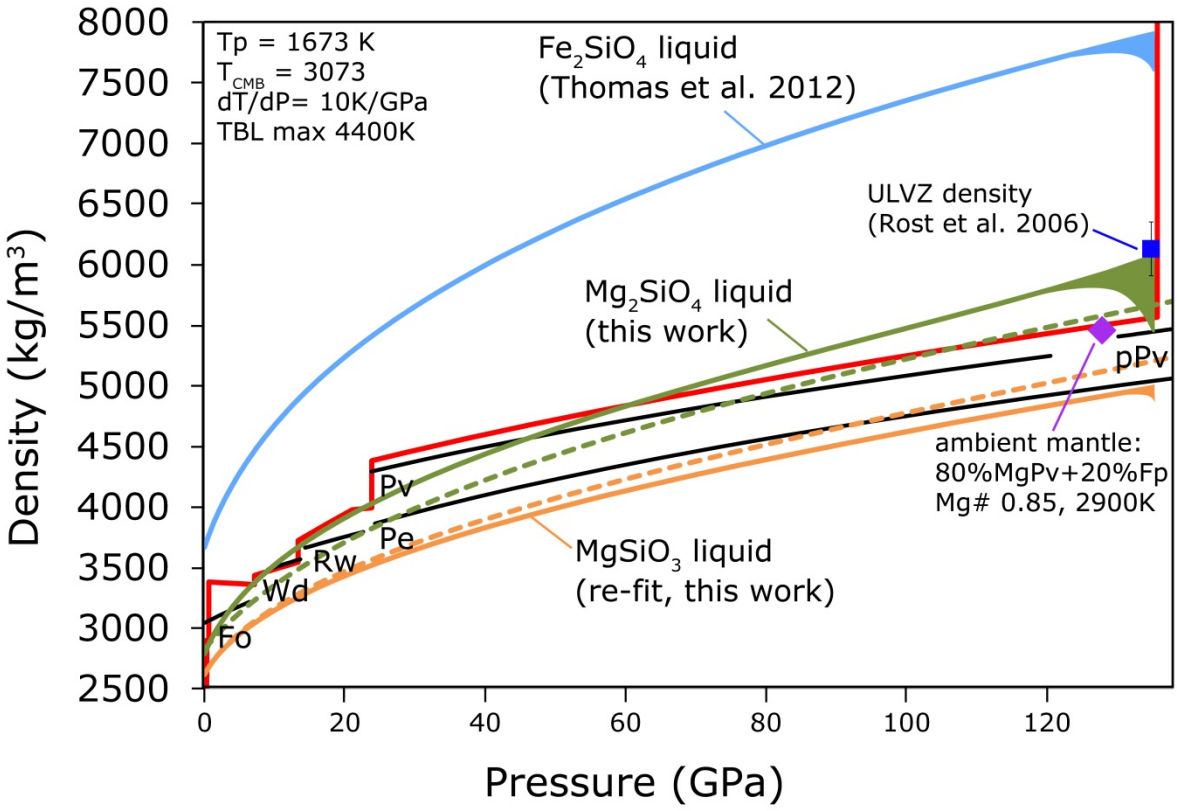

Figure 8

Figure 7

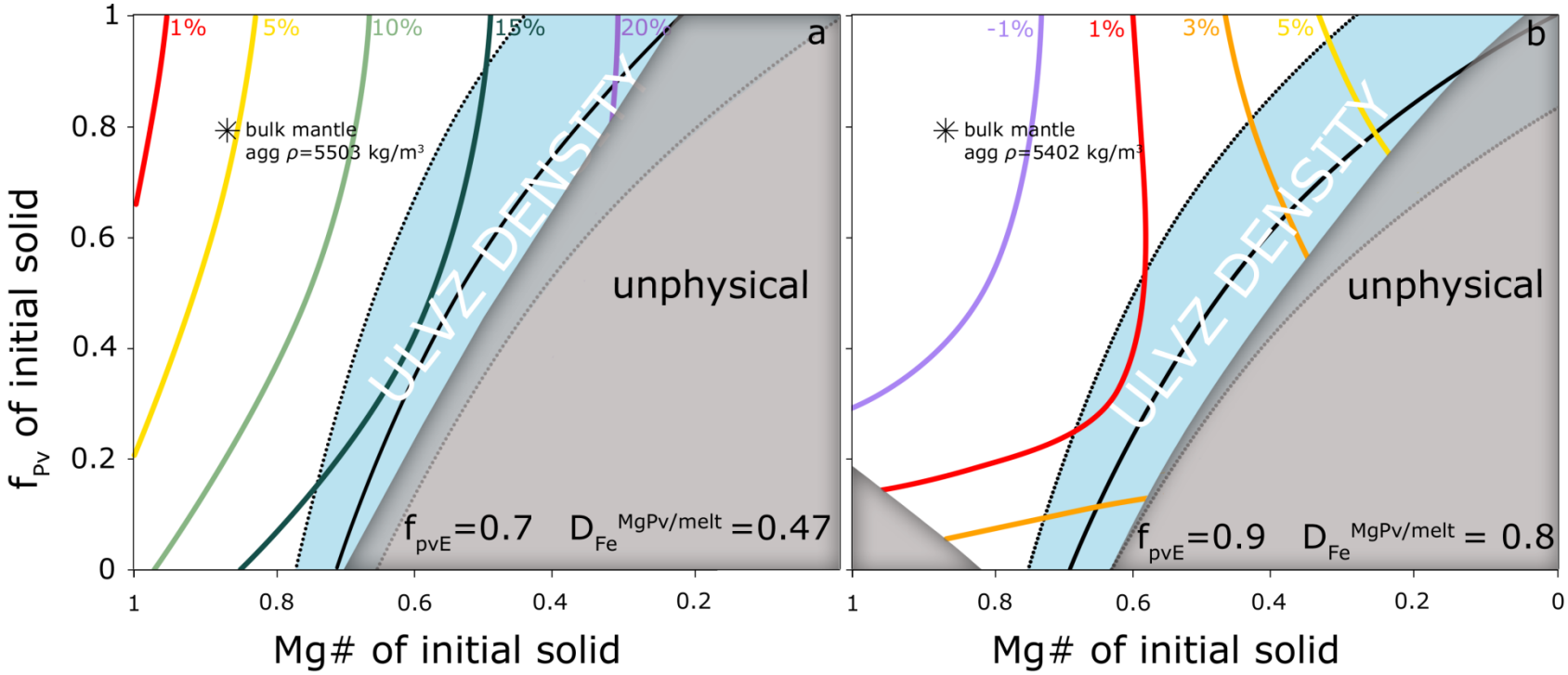
1%
5%
10%
15%
20%
a
bulk mantle
agg ρ=5503 kg/m³
ULVZ DENSITY
unphysical
f_pvE=0.7 D_Fe^MgPv/melt=0.47
-1%
1%
3%
5%
b
bulk mantle
agg ρ=5402 kg/m³
ULVZ DENSITY
unphysical
f_pvE=0.9 D_Fe^MgPv/melt = 0.8
f_Pv of initial solid
Mg# of initial solid
Mg# of initial solid
1
0.8
0.6
0.4
0.2
0

Figure 9